Front. Earth Sci. 2023, 17(1): 230–250
https://doi.org/10.1007/s11707-022-1018-x

RESEARCH ARTICLE

Geochemistry of rare earth elements and yttrium in Late Permian coals from the Zhongliangshan coalfield, southwestern China

Qingfeng LU[1,2,3], Shenjun QIN (✉)[2], Hongyang BAI[1,3], Wenfeng WANG (✉)[1,3], De'e QI[2], Xin HE[1,3], Bofei ZHANG[1,3]

1 School of Resources and Geosciences, China University of Mining & Technology, Xuzhou 221116, China
2 Key Laboratory for Resource Exploration Research of Hebei Province, Hebei University of Engineering, Handan 056038, China
3 Key Laboratory of Coalbed Methane Resources & Reservoir Formation Process, Ministry of Education, China University of Mining & Technology, Xuzhou 221008, China

Abstract Rare earth elements and yttrium (REY) in coal deposits are considered promising alternative sources for these resources owing to their increasing global demand. This paper reports the geochemical characteristics of REY in the Late Permian coals from an underground K1a seam section of the Zhongliangshan coalfield in Chongqing, southwestern China. The mineralogy, degree of enrichment, distribution patterns, modes of occurrence, and sediment origin of REY were investigated. Compared with the average of world coals, the concentration of REY in the K1a coals were normal, dominated by light REY (LREY), with less medium and heavy REY (MREY, HREY). The fractionation degree of the MREY and HREY are higher than that of LREY in most K1a coal samples, deduced from the mixed enrichment type of REY, mainly including M-H-type, and a few L-M type and H-type. In addition, the combination of anomalies of Ce, Eu, Gd, and Al_2O_3/TiO_2 parameters, the terrigenous materials in the K1a coal were derived from the felsic-intermediate rocks at the top of the Emeishan basalt sequence, and the samples were affected by seawater intrusion during early peat accumulation. Although the minerals primarily consist of kaolinite, illite, pyrite, and small amounts of quartz, calcite and anatase, REY are correlated with ash yield, SiO_2, and Al_2O_3, revealing that the REY mainly occur in aluminosilicate minerals, especially kaolinite and illite. Meanwhile, REY positively relate to P_2O_5 and Zr, which may exist in phosphate-containing minerals or zircon. Furthermore, most samples in the K1a coal or ash do not reach the cut-off grade for the beneficial recovery of REY. With the exception of central Guizhou, southwestern Chongqing, and the junction of western Guizhou and northeastern Yunnan, the REY content in coals from southwestern China are high, and its by-products are suitable as potential REY sources.

Keywords rare earth elements and yttrium, Zhongliangshan K1a coal, sediment source, modes of occurrence, geochemical characteristics

1 Introduction

Coal deposits can contain abundant valuable trace or major elements with potential utilized economic value, such as U, Ge, Ga, Li, rare earth elements and yttrium (REY), platinum group elements (PGEs), and Al (Dai et al., 2010a, 2016a, 2018, 2020, 2021; Seredin and Dai, 2012; Qin et al., 2015a, 2015b, 2018a; Sun et al., 2016; Ma et al., 2020; Xu et al., 2022). Uranium has been successfully extracted from coal for nuclear applications by the Soviet Union and the United States since the World War Second II (Kislyakov and Shchetochkin, 2000). The Lincang coal in Yunnan, and Wulantuga coal in Inner Mongolia, are two typical large germanium coal deposits with independent industrial mining values (Zhuang et al., 2006; Hu et al., 2009; Dai et al., 2012a, 2015a, 2018), with tons of germanium being obtained from both coal mines. Ge-rich coal deposits are currently utilized as raw materials for Ge in China and Russia (Dai et al., 2014a). Aluminum and gallium have also been successfully extracted from coal and coal ash from the Jungar coalfield, China (Qin et al., 2015a; Sun et al., 2016). The extraction of lithium from coal fly ash is still

Received March 24, 2022; accepted April 15, 2022

E-mail: qinsj528@hebeu.edu.cn (Shenjun QIN)
wangwenfeng@cumt.edu.cn (Wenfeng WANG)

in the experimental stage (Qin et al., 2015b; Li et al., 2020a). The rare earth elements and yttrium are widely used in permanent magnets, batteries, phosphors, catalysts, etc (Hower et al., 2016). REY as an important strategic resource, and its worldwide demand is increasing, especially in China, Russia, US, and Japan (accounting for more than 80%). The high REY contents in coals were first studied by Goldschmidt and Peters (1933). High concentrations of REY in coal ash (from 0.2% to 0.3%) were discovered in the Russian Far East coal basins, and a possible recovery suggestion for REY was proposed (Seredin, 1991).

The REY are the general term for lanthanides and yttrium in group IIIB of the periodic table. In this study, REY were used to represent 15 elements, including La, Ce, Pr, Nd, Sm, Eu, Gd, Tb, Dy, Y, Ho, Er, Tm, Yb, and Lu. As Y^{3+} (89.3×10^{-12} m) and Ho^{3+} (89.4×10^{-12} m) have very similar ionic radii and the same ionic charge, Y^{3+} can be placed between Ho^{3+} and Dy^{3+} for the REY normalized distribution pattern analysis (Dai et al., 2016a). The classifications of REY are different according to diverse geochemical and economic perspectives. Twofold (LREY, HREY) and threefold (LREY, MREY, HREY) classifications are common classification schemes from a geochemical perspective. The threefold classification is more convenient than the twofold classification for analyzing the REY distribution (Seredin and Dai, 2012). In addition, REY can be classified into critical (Nd, Eu, Tb, Dy, Y, and Er), uncritical (La, Pr, Sm, and Gd), and excessive (Ce, Ho, Tm, Yb, and Lu) elements when evaluating coal deposits as potential raw REY sources (Seredin, 2010).

REY distribution patterns have been widely used to determine the origin and differentiation of igneous rocks, as well as certain sedimentary rocks (Seredin, 1996; Dai et al., 2016a). In general, the REY in coals are normalized to some standard materials to identify its fractionation, i.e., chondrite (Zhao et al., 2012), Upper Continental Crust (UCC, Taylor and McLennan, 1985), Post-Archaean Australian Shale (PAAS, Taylor and McLennan, 1985), North American Shale Composite (NASC, Gromet et al., 1984), and coal itself (Finkelman, 1993). Of course, the standard materials used for REY normalization should preferably have a similar origin to that of the coal. The normalization of REY in coal to UCC is becoming more widely accepted because coal was deposited within the UCC, and mixed with detrital UCC input during the peat stage of coal formation (Dai et al., 2016a). The redox-sensitive elements Ce and Eu, and non-redox-sensitive Gd, may be anomalous in coals and associated host rocks in certain circumstances. The characteristics of Ce, Eu, and Gd in coal are influenced by the rocks in the sediment source region and hydrothermal fluids, and are possibly related to the seawater, groundwater, etc. (Elderfield and Greaves, 1982; Eskenazy, 1987a,1987b; Bau, 1991; Bau et al., 2014; Dai et al., 2015c, 2016a). Therefore, the geochemical parameters of REY, such as Ce, Eu, and Gd anomalies can be used to identify the sediment source region and sedimentary environment (Eskenazy, 1987a, 1987b; Dai et al., 2013, 2016a).

Southwest China contains abundant coal resources, with coal ranks from lignite to anthracite, and the coal-accumulation period including Early Carboniferous (C_1), Late Permian (P_2), Early and Late Triassic (T_1, T_2), and Neogene (N). Reports on coals from southwestern China mainly focus on mineralogy, petrology, organic and elemental geochemistry, environment issue, etc. Initially, many scholars were attracted to the hazardous elements in coals of southwestern China, i.e., As, Co, Hg, Cr, V, and S (Ding et al., 1999; Dai et al., 2012b; Duan et al., 2017; Zhao et al., 2017). Owing to the continuous changes in the relationship between the supply and demand of rare metals, the valuable metals in coal or coal by-products, such as Ge, Li, and REY, have gradually gained attention (Dai et al., 2015a, 2018; Duan et al., 2019; Wang et al., 2019; Liu et al., 2019, 2020; Li et al., 2021). The Zhongliangshan coal is located in Chongqing, southwestern China, and is characterized by low-medium ash and medium-high sulfur content. The mineralogical, petrological, gasification, toxic and beneficial trace elements, and organic geochemical characteristics of the Zhongliangshan coal have been reported, however, there is a dearth of detailed analysis on rare earth elements (Xin et al., 2017; Qin et al., 2018b, 2018c; Zou et al., 2018). Therefore, the Zhongliangshan coal was chosen for investigation in this study, to analyze its enrichment, modes of occurrence, distribution patterns, and sediment source. In addition, the potential of coal or coal by-products from the Zhongliangshan coalfield and parts of southwestern China were evaluated as potential raw materials for rare earth elements and yttrium.

2 Geological setting

Five coalfields, including the Zhongliangshan, Tianfu, Yongrong, Songzao, and Nantong coalfields, constitute important coal resource production bases of Chongqing, southwest China (Fig. 1). The Zhongliangshan coalfield is located approximately 18 km from downtown Chongqing, with a total area 4.7 km^2 and divided into two mining areas: the southern mine and northern mines. In this study, samples from the Zhongliangshan northern mine were investigated and analyzed.

The newest and oldest strata exposed in this coalfield are the Late Triassic Xujiahe Formation and Early Permian Maokou Formation, respectively. The coal-bearing sequence is the Late Permian Longtan Formation (P_2l). The Longtan Formation is integrated under the Late Permian Changxing Formation (P_2c) and unconformably overlies the Early Permian Maokou Formation (P_1m)

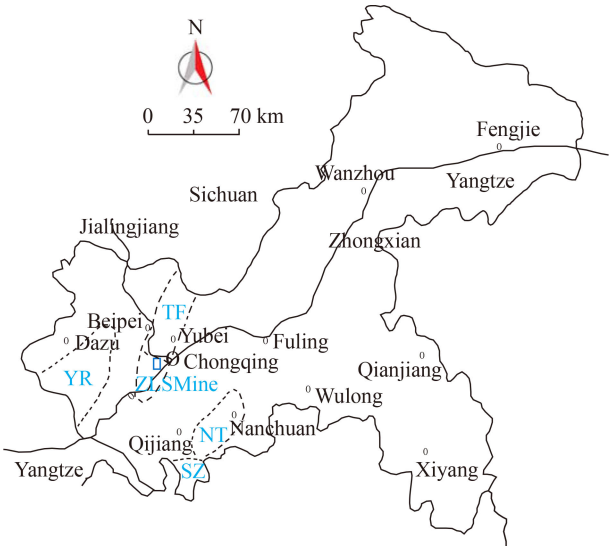

Fig. 1 Location of five coalfields (ZLS, Zhongliangshan; TF, Tianfu; YR, Yongrong; SZ, Songzao; NT, Nantong).

(Fig. 2). The Longtan Formation mainly consists of gray mudstone, silty mudstone, pelitic siltstone, claystone, argillaceous limestone, fine sandstone, and coal seams. From bottom to top, tuff, argillaceous limestone, limestone, and mudstone serve as four marker beds for the coal-bearing strata (named I1 to I4). Meanwhile, brachiopods, ferns, cephalopods, lamellibranches, trilobites, and other fossils occur within the Longtan Formation (Zou et al., 2018). The sedimentary environment of the Longtan Formation is a paralic continental-marine transitional environment. The coal bearing sections (first and second sections) of the Longtan Formation, with an average thickness of 71.46 m, contain 10 coal seams (numbered K1–K10 from top to bottom) (Fig. 2). These coal seams can be divided into five full-area mineable seams (K1, K2, K3, K9, and K10), three minable seams (K4, K5, and K7), one locally minable seam (K8), and one unminable seam (K6). The K1 seam is located at the top of the second coal-bearing section and contains two parting layers, forming three independent coal layers (K1a, b, and c), with average thicknesses of 1.64 m (0.33 m) 0.58 m (1.29 m) 0.38 m, respectively. The coal samples were dominated by bright coal, followed by dark coal, and entrained thin strips of vitrinite. The roof and floor of the K1 seam are dark gray iron-bearing mudstone and gray claystone, respectively.

3 Samples and analytical methods

A total of 23 samples were collected from an underground working face in the K1a coal seam of the Zhongliangshan coalfield following the GB/T 482-2008 (2008) Chinese Standard method. The samples contained one roof (marked with R), one parting (marked with P), and 20-one coals (numbered as ZLS-1 to ZLS-21 from top to bottom) (Fig. 2). Each sample was obtained over an area that was 10 cm wide, 10 cm deep and 10 cm thick. All collected samples were immediately stored in plastic bags to minimize contamination and oxidation. The samples were ground and passed through 40-mesh and 200-mesh sieves in the sample preparation laboratory for subsequent geochemical analysis.

Proximate (i.e., moisture, ash, and volatile matter) and sulfur (i.e., total sulfur, and forms of sulfur) analysis were conducted following the ASTM Standards D3173-11 (2011), D3174-11 (2011), D3175-11 (2011), D3177-02 (2002), and D2492-02 (2002), respectively. The coal samples were characterized by low moisture (0.88%), medium volatile matter on a dry and ash-free basis (22.53%), and low-medium ash on a dry basis (15.06%, ranging from 9.07% to 31.75%). The coal samples were classified as medium-high sulfur coal, because the average total sulfur content was 2.61% (varies from 0.81% to 7.75%). Meanwhile, the dominant forms of sulfur were pyritic (1.61%) and organic (0.77%). The total sulfur contents are high in ZLS-1 (7.16%), ZLS-18 (7.75%), and ZLS-19 (7.05%), because more pyrite existed in these coal samples (the pyritic sulfur contents were 4.19%, 5.26%, and 4.90%, respectively) (Table S1).

The mineral compositions of the coal samples were obtained by optical microscopy (Leica DM2500P), low-temperature oxygen plasma ashes-X-ray diffraction (LTA-XRD, Quorum K1050X-D/Rigaku MAX2200PC), and scanning electron microscopy-energy dispersive spectrometer (SEM-EDS, Hitachi SU8220). XRD testing was performed on the 200-mesh coals after they were completely ashed in the LTA. The XRD scan was conducted over 2θ angle ranging from 5° to 70°, with a step size of 0.02°. Siroquant^{TM} was used to quantitatively determine the mineral composition of the coal LTAs. The 40-mesh coals were formed into coal bricks using epoxy resin and curing agent. After grinding and polishing the coal brick, the minerals were observed using an optical microscope (Leica DM2500P) under the oil-reflected light. Besides, coal bricks were sprayed with gold under dry conditions. The mineral morphology and elemental compositions in the coals were determined by SEM-EDS, with working distance of 7–20 mm, beam voltage of 20 kV, and current of 5 μA.

The 200-mesh coals were ashed at 815°C in a muffle furnace, then the ashes were analyzed to determine the major elemental oxides by X-ray fluorescence spectrometry (XRF, Thermo Fisher Scientific ARL9800). The REY concentrations in the samples were determined using inductively coupled plasma mass spectrometry (ICP-MS, Thermal Elemental X-II), with the exception of Pm. The samples were digested in an UltraClave microwave high-pressure reactor; 40 mg coal was digested at 150°C using three reagents (1.5 mL 68% HNO_3, 0.5 mL 40% HF, and 1.5 mL 50% $HClO_4$) in PTFE vessels. The

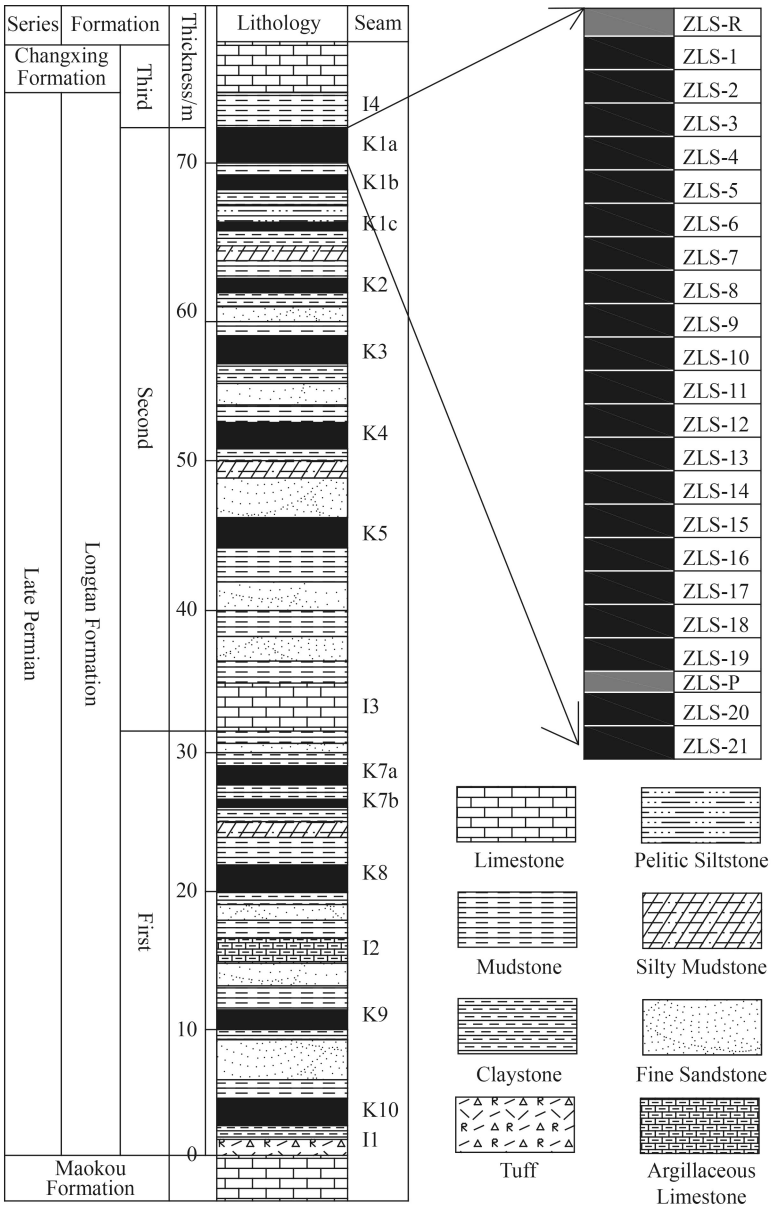

Fig. 2 Stratigraphic column of the Late Permian Longtan Formation from the Zhongliangshan, Chongqing.

digestion solution was then transferred to PFEP bottles, and diluted to 50 g using 2% HNO_3.

4 Results

4.1 Mineralogy

The minerals in the LTAs of the K1a coal were identified from X-ray diffraction patterns, and the quantitative data of the minerals are listed in Table 1. The mineralogy is dominated by kaolinite, illite, illite/smectite mixed layer, and pyrite, with traces of quartz, calcite, and anatase. Kaolinite primarily occurs in collodetrinite as cell-fillings (Fig. 3(a)) and rounded fine particles (Fig. 3(b)), and has a lamellar structure under high magnification (Fig. 3(c)). Pyrite shows framboidal (Figs. 3(d) and 3(h)), cell-filling (Fig. 3(e)), fracture-filling (Fig. 3(f)), dispersed crystals and large euhedral cubes (Figs. 3(g) and 3(h)) structures in the K1a coal. Cell-filling and fracture-filling pyrite in coal were formed by low-temperature hydrothermal fluids during the epigenetic stage (Duan et al., 2019). Calcite occurs as fracture-fill and cavity-fill structures with collotelinite, indicating epigenetic and syngenetic genesis, respectively (Figs. 3(i) and 3(j)), which are mostly related to the activity of hydrothermal fluids and the precipitation of rich Ca^{2+} solutions in the cavities during the diagenesis process. A small amount of quartz was observed in the coals, and distributed in collodetrinite or collotelinite with a particle size of approximately 5–10 μm (Fig. 3(k)), reflecting an authigenic origin. The content of anatase is high in ZLS-17, which can be confirmed by the

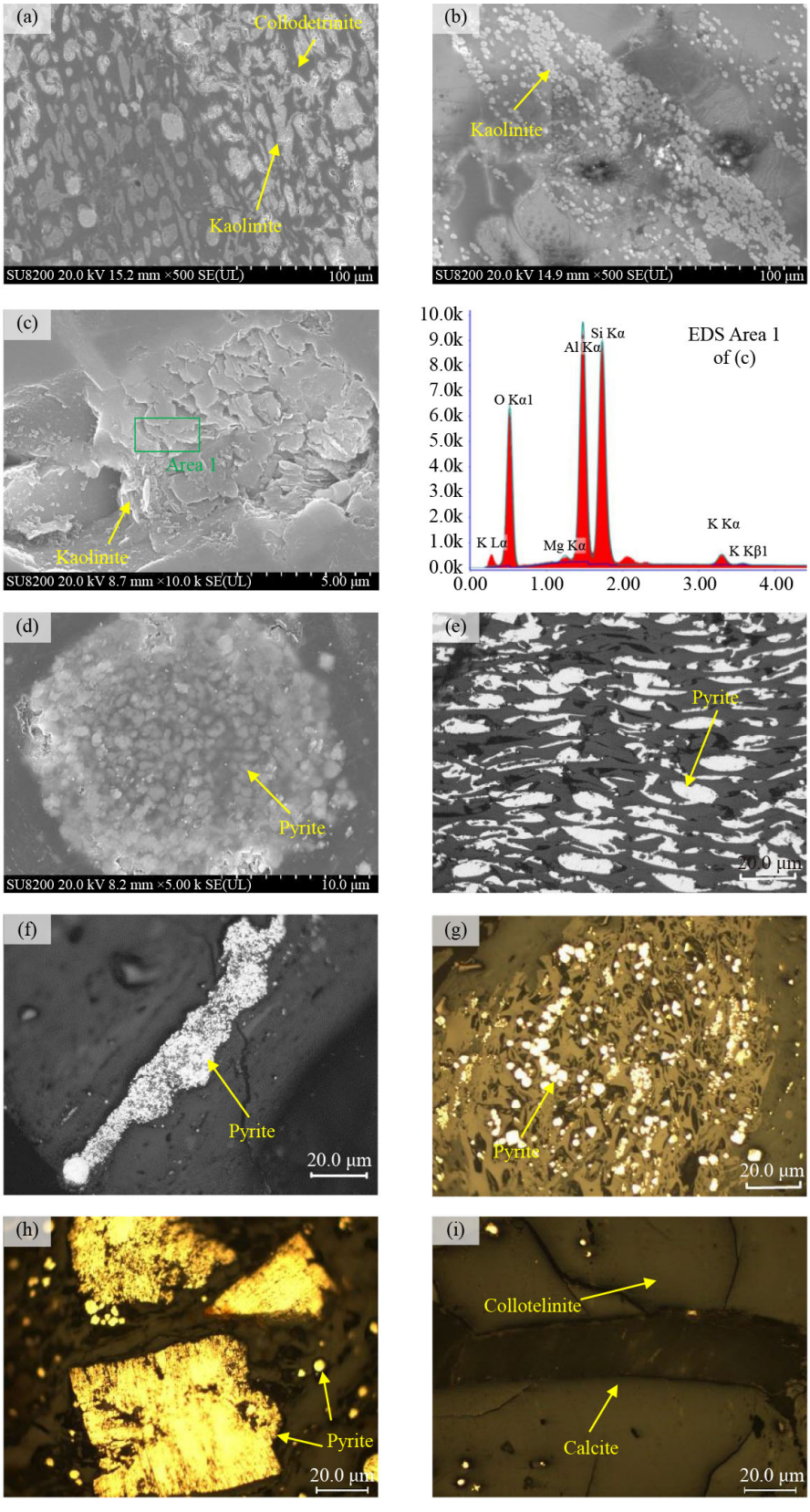
(a)
Collodetrinite
Kaolinite
SU8200 20.0 kV 15.2 mm ×500 SE(UL)
100 μm
(b)
Kaolinite
SU8200 20.0 kV 14.9 mm ×500 SE(UL)
100 μm
(c)
Area 1
Kaolinite
SU8200 20.0 kV 8.7 mm ×10.0 k SE(UL)
5.00 μm
10.0k
9.0k
8.0k
7.0k
6.0k
5.0k
4.0k
3.0k
2.0k
1.0k
0.0k
O Kα1
Si Kα
Al Kα
K Lα
Mg Kα
K Kα
K Kβ1
0.00
1.00
2.00
3.00
4.00
EDS Area 1
of (c)
(d)
Pyrite
SU8200 20.0 kV 8.2 mm ×5.00 k SE(UL)
10.0 μm
(e)
Pyrite
20.0 μm
(f)
Pyrite
20.0 μm
(g)
Pyrite
20.0 μm
(h)
Pyrite
20.0 μm
(i)
Collotelinite
Calcite
20.0 μm

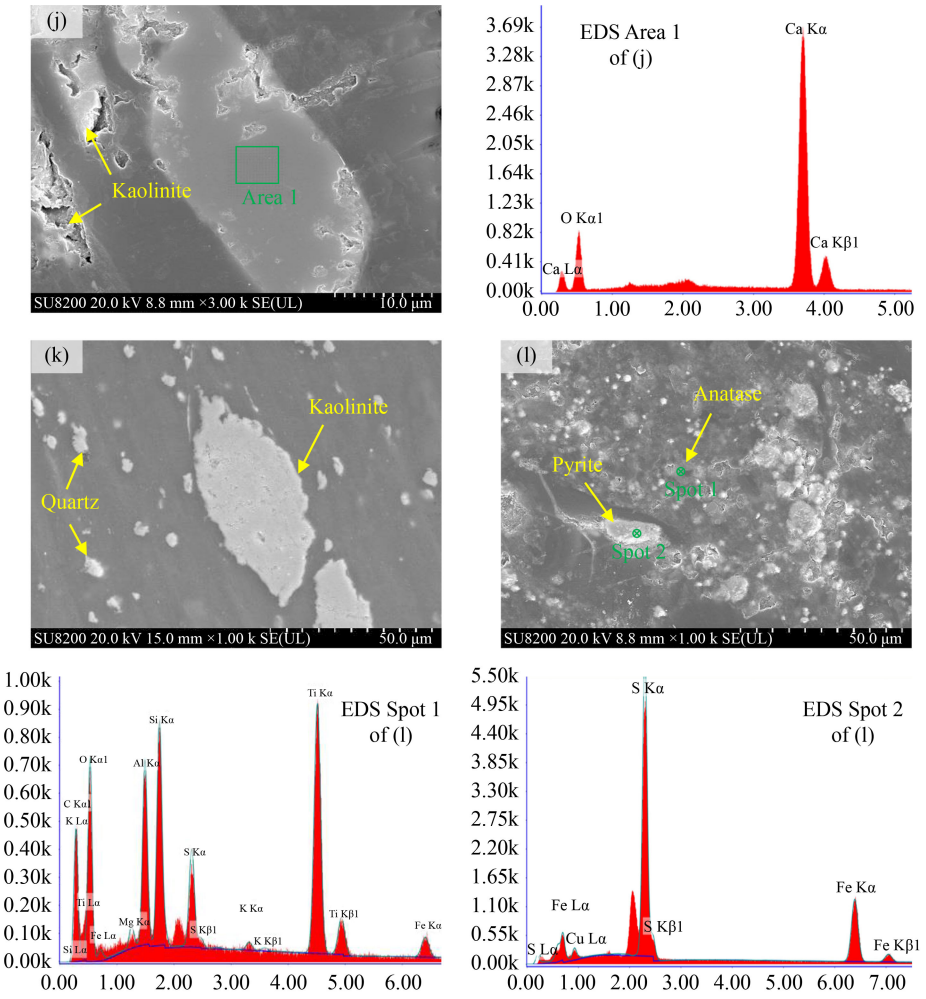

Fig. 3 Minerals in the Zhongliangshan K1a coal.

Table 1 The proportions of minerals in the Zhongliangshan coal LTAs (%)

Samples	Kaolinite	Illite+I/S	Quartz	Calcite	Pyrite	Anatase
ZLS-R	10.6	52.5	11.2	3.3	18.2	4.2
ZLS-1	34.3		18.3	17	27.1	3.3
ZLS-3	62.2		11.6	9.9	13.7	2.6
ZLS-7	75.7		4.2	11.5	8.6	
ZLS-9	35.9	54.4	1.4	1.9	6.4	
ZLS-13	57.2	39.8		2.7	0.3	
ZLS-17	39.5	35.7		2	9.8	13.0
ZLS-18	33.4	44		4	15.6	3.1
ZLS-P	51	35.1		0	6.3	7.6
ZLS-21	55.7	26.7		8.4	6.5	2.8

observation of anatase in ZLS-17 coal under the SEM-EDS (Fig. 3(l)).

4.2 Concentration and enrichment of REY

The concentrations of rare earth elements and yttrium in the K1a coal, as well as those for average world coals, are presented in Table 2. The results show that the total REY concentrations in the K1a coal range from 39.28 to 125.4 μg/g, with an average of 77.18 μg/g. The average concentration of REY in the K1a coal is slightly higher than that in world coal (68.5 μg/g, Ketris and Yudovich,

Table 2 Concentration of rare earth elements and yttrium in the ZLS K1a coal (μg/g)

Samples	LREY					MREY					HREY					Sum
	La	Ce	Pr	Nd	Sm	Eu	Gd	Tb	Dy	Y	Ho	Er	Tm	Yb	Lu	
ZLS-R	37.46	70.03	8.55	36.83	7.24	1.52	5.67	0.68	3.31	16.00	0.65	1.76	0.25	1.58	0.28	191.8
ZLS-1	18.04	33.58	3.74	16.95	3.09	0.63	2.76	0.36	1.94	10.94	0.42	1.18	0.19	1.15	0.20	95.17
ZLS-2	16.00	28.33	2.55	13.59	2.86	0.49	2.52	0.33	1.87	9.36	0.37	1.08	0.16	1.05	0.17	80.73
ZLS-3	10.17	18.91	2.11	9.38	1.87	0.34	1.85	0.27	1.50	9.74	0.31	0.84	0.13	0.75	0.12	58.29
ZLS-4	7.70	16.88	1.24	7.97	1.57	0.30	1.58	0.26	1.45	10.00	0.30	0.90	0.13	0.76	0.13	51.17
ZLS-5	6.43	11.46	1.25	5.72	1.22	0.23	1.39	0.24	1.47	10.27	0.32	0.90	0.14	0.85	0.14	42.03
ZLS-6	6.58	11.26	1.21	5.52	1.20	0.22	1.32	0.23	1.33	9.59	0.30	0.83	0.12	0.80	0.13	40.64
ZLS-7	6.36	11.23	1.24	5.40	1.11	0.20	1.28	0.22	1.29	8.84	0.29	0.79	0.13	0.77	0.13	39.28
ZLS-8	10.87	16.59	1.87	8.70	1.86	0.32	1.86	0.29	1.69	9.45	0.36	0.99	0.16	0.96	0.15	56.12
ZLS-9	13.06	28.31	2.76	11.70	2.19	0.38	2.12	0.31	1.80	10.96	0.41	1.13	0.18	1.16	0.18	76.65
ZLS-10	11.24	21.53	2.03	9.25	0.99	0.36	1.92	0.30	1.57	10.24	0.40	1.02	0.16	0.90	0.15	62.06
ZLS-11	8.95	17.10	1.94	8.72	1.75	0.34	1.79	0.27	1.56	11.18	0.33	0.91	0.14	0.83	0.14	55.95
ZLS-12	9.36	21.57	2.37	9.37	2.12	0.40	1.90	0.29	1.56	10.57	0.37	0.96	0.15	0.90	0.15	62.04
ZLS-13	14.98	26.75	2.96	12.91	2.39	0.42	2.22	0.29	1.55	10.97	0.33	0.95	0.14	0.89	0.15	77.9
ZLS-14	13.26	25.26	2.86	11.29	2.40	0.47	2.24	0.30	1.64	11.24	0.32	0.93	0.14	0.81	0.14	73.3
ZLS-15	11.68	22.34	2.63	11.96	2.44	0.50	2.31	0.33	1.74	12.85	0.35	0.95	0.15	0.82	0.14	71.19
ZLS-16	20.37	28.97	3.03	19.56	3.06	0.57	3.03	0.42	2.37	13.70	0.46	1.24	0.19	1.00	0.16	98.13
ZLS-17	24.51	43.91	4.79	21.20	3.87	0.89	3.71	0.49	2.52	15.99	0.51	1.38	0.21	1.20	0.20	125.4
ZLS-18	20.33	40.24	4.57	21.00	4.03	1.00	4.02	0.60	3.03	21.24	0.63	1.86	0.26	1.57	0.24	124.6
ZLS-19	16.79	34.35	4.30	20.45	4.25	1.12	4.43	0.63	3.65	26.34	0.75	2.08	0.30	1.69	0.28	121.4
ZLS-P	18.27	30.24	3.02	19.24	3.96	1.00	4.24	0.62	3.02	28.24	0.71	2.02	0.25	1.29	0.28	116.4
ZLS-20	15.69	31.87	3.85	18.26	3.89	0.98	4.22	0.61	3.58	30.19	0.78	2.09	0.31	1.72	0.28	118.3
ZLS-21	15.24	29.55	2.24	11.02	3.02	0.27	3.06	0.52	2.35	21.26	0.24	1.20	0.20	0.46	0.12	90.75
Av.1	13.22	24.76	2.64	12.38	2.44	0.50	2.45	0.36	1.97	13.57	0.41	1.15	0.17	1.00	0.16	77.18
Av.2	27.86	50.13	5.79	28.03	5.60	1.26	4.95	0.65	3.17	22.12	0.68	1.89	0.25	1.43	0.28	154.1
World	11	23	3.5	12	2	0.47	2.7	0.32	2.1	8.4	0.54	0.93	0.31	1	0.2	68.47

Notes: World, average concentration of trace elements in world coal; Av.1, average concentration of coal samples in the K1a coal; Av.2, average concentration of roof and parting.

2009). With the exception of Pr, Gd, Dy, Ho, Tm, and Lu, the concentrations of other rare earth elements and yttrium in the K1a coal were higher than the corresponding background average values of world coals. The total concentrations of REY in the roof and parting were 191.8 μg/g and 116.4 μg/g, which were higher than that in all coal samples except ZLS-17 to ZLS-20. In this study, REY were analyzed using the threefold geochemical classification, including light (LREY, La–Sm), medium (MREY, Eu–Y), and heavy (HREY, Ho–Lu) REY. The REY in the K1a coals were dominated by LREY (av. 55.44 μg/g), followed by MREY (av. 18.85 μg/g). The HREY concentrations are low, varying from 2.11 to 5.18 μg/g (av. 2.90 μg/g) (Fig. 4). The variations of REY content have three significantly increased peaks observed in the Zhongliangshan samples, i.e., ZLS-R, ZLS-9, and ZLS-17 to ZLS-19 (Fig. 5). The content of individual element in the K1a samples has a coincident distribution trend (Fig. 5), because of the fact that these elements have similar ionic radii, geochemical behaviors, and chemical stabilities (Qin et al., 2018a), indicating that the modes of occurrence, affinity, and genesis of each REY in the Zhongliangshan coal are uniform.

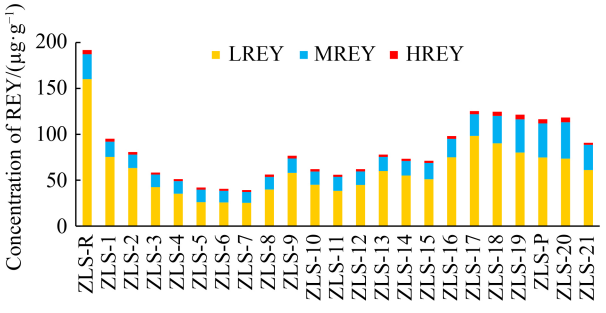

Fig. 4 Concentration distribution of LREY, MREY, and HREY in the ZLS K1a coal.

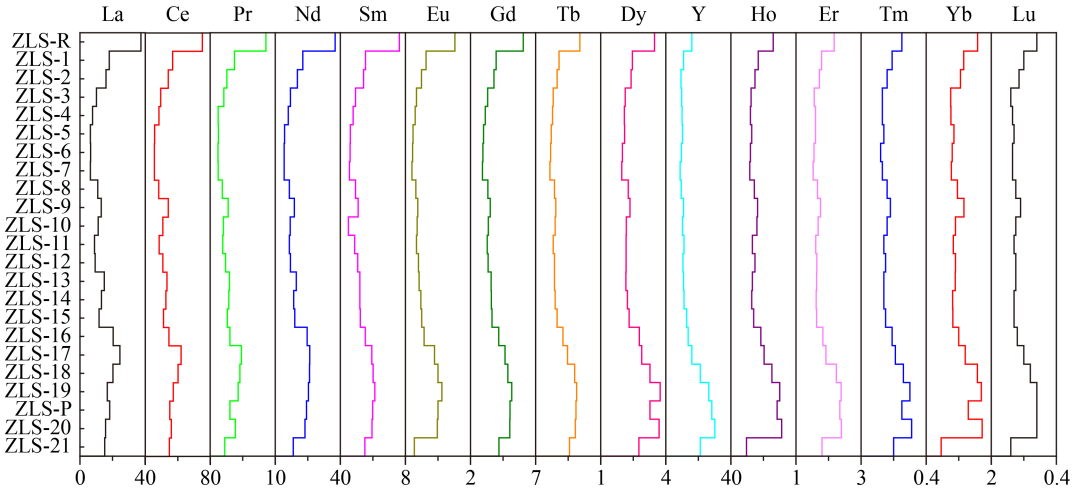

Fig. 5 Vertical distribution of REY in the ZLS K1a coal (μg/g).

Based on the concentration coefficient (CC, the ratio of elemental concentration in investigated coal to that for average world coal, Dai et al. (2015b)), the REY concentrations can be seperated into six categories: depleted (CC < 0.5), normal (0.5 ⩽ CC < 2), slightly enriched (2 ⩽ CC < 5), enriched (5 ⩽ CC < 10), significantly enriched (10 ⩽ CC < 100), and anomalously enriched (CC ⩾ 100). For the K1a coal, all rare earth elements and yttrium had a normal level, with 0.5 < CC < 2 (Fig. 6). The concentration coefficients for La in ZLS-17 (2.23), Sm and Eu in ZLS-18 (2.02, 2.13) and ZLS-19 (2.13, 2.38) were slightly enriched. In addition, the concentrations of REY in the roof and parting were higher than those in the coals. The elements La, Ce, Nd, Sm, Eu, Tb, and Y were slightly enriched in the roof and parting samples, while the other elements were at a normal level.

4.3 Geochemical characteristics of REY

The geochemical parameters and distribution patterns of rare earth elements and yttrium can be used as geochemical indicators for tracing the coal-forming source and sedimentary environment of coal deposits. The geochemical parameters, i.e., LREY/MREY, LREY/HREY, MREY/HREY, La_N/Lu_N, La_N/Sm_N, Gd_N/Lu_N, enrichment types, La_N/Yb_N, Ce anomaly (Ce_N/Ce_N*), Eu anomaly (Eu_N/Eu_N*), and Gd anomaly (Gd_N/Gd_N*) were calculated (Table 3). The distribution patterns of REY in the K1a coal were shown in Fig. 7. The rare earth elements and yttrium were normalized to the Upper Continental Crust (UCC) in this study (Taylor and McLennan, 1985).

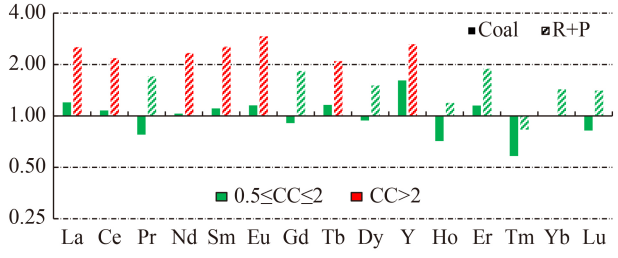

Fig. 6 Concentration coefficients (CC) of REY in the ZLS K1a samples.

The values of LREY/HREY and LREY/MREY are higher than 1 in the K1a coal, with an average of 19.11 and 3.02 (Table 3), indicating that the rare earth elements have a high fractionation degree. This may be attributed to the heavy rare earth elements being more likely to migrate out of the coal-forming swamp when it is invaded by seawater (Qin et al., 2018a). The ratio of La_N to Yb_N can reflects the fractionation between LREY and HREY. The ratio values of La_N to Yb_N are low than 1 in most samples, i.e., ZLS-3 to ZLS-12, and ZLS-18 to ZLS-20, indicating that the HREY has a higher fractionation than LREY in most coal samples. The other samples presented a high degree of LREY fractionation.

Corresponding to their classification, three enrichment types of REY are found in coal: light (L-type, $La_N/Lu_N > 1$), medium (M-type, $La_N/Sm_N < 1$, $Gd_N/Lu_N > 1$), and heavy (H-type, $La_N/Lu_N < 1$) REY types (Seredin and Dai, 2012). The K1a coals are primarily enriched in mixed M-type (the average values of La_N/Sm_N and Gd_N/Lu_N are 0.85 and 1.23) and H-type (the average value of La_N/Lu_N is 0.85) (Table 3), reflecting that the MREY and HREY are more enriched than LREY in the K1a coal. The H-type enrichment was likely due to hydrothermal intrusion, whereas the M-type enrichment may be related to natural waters (Wang et al., 2016). Specifically, the REY of the K1a coal has three enrichment types, including M-H-type (ZLS-1, ZLS-3 to ZLS-4, ZLS-8, ZLS-11 to ZLS-12, ZLS-15, ZLS-18 to ZLS-20), H-type (ZLS-5 to ZLS-7, ZLS-9 to ZLS-10), and L-M-type (ZLS-2, ZLS-13 to ZLS-14, ZLS-16 to ZLS-17, ZLS-21).

The Ce, Eu, and Gd anomalies were calculated as

Table 3 Geochemical parameters of rare earth elements and yttrium in the ZLS K1a coal

Samples	$\frac{LREY}{MREY}$	$\frac{LREY}{HREY}$	$\frac{MREY}{HREY}$	$\frac{La_N}{Lu_N}$	$\frac{La_N}{Sm_N}$	$\frac{Gd_N}{Lu_N}$	Type	$\frac{La_N}{Yb_N}$	$\frac{Ce_N}{Ce_N^*}$	$\frac{Eu_N}{Eu_N^*}$	$\frac{Gd_N}{Gd_N^*}$
ZLS-R	5.89	35.42	6.01	1.43	0.78	1.71	L-M	1.74	0.89	1.21	1.20
ZLS-1	4.53	24.01	5.30	0.96	0.88	1.16	M-H	1.15	0.93	1.11	1.20
ZLS-2	4.35	22.38	5.15	1.01	0.84	1.25	L-M	1.12	0.99	0.93	1.19
ZLS-3	3.10	19.74	6.37	0.90	0.82	1.30	M-H	0.99	0.93	0.93	1.16
ZLS-4	2.60	15.93	6.12	0.63	0.74	1.02	M-H	0.74	1.22	0.93	1.07
ZLS-5	1.92	11.10	5.79	0.49	0.79	0.84	H	0.55	0.92	0.86	1.07
ZLS-6	2.03	11.82	5.82	0.54	0.82	0.86	H	0.60	0.90	0.84	1.06
ZLS-7	2.14	12.01	5.61	0.52	0.86	0.83	H	0.61	0.91	0.82	1.08
ZLS-8	2.93	15.23	5.19	0.77	0.88	1.04	M-H	0.83	0.83	0.85	1.11
ZLS-9	3.73	18.96	5.09	0.77	0.89	0.99	H	0.83	1.07	0.89	1.15
ZLS-10	3.13	17.13	5.47	0.80	1.70	1.08	H	0.92	1.02	1.35	1.31
ZLS-11	2.54	16.37	6.44	0.68	0.77	1.08	M-H	0.79	0.93	0.97	1.15
ZLS-12	3.04	17.70	5.82	0.67	0.66	1.07	M-H	0.76	1.04	0.98	1.09
ZLS-13	3.88	24.39	6.28	1.07	0.94	1.25	L-M	1.23	0.91	0.94	1.22
ZLS-14	3.47	23.53	6.79	1.01	0.83	1.35	L-M	1.20	0.93	1.04	1.20
ZLS-15	2.88	21.18	7.36	0.89	0.72	1.39	M-H	1.04	0.92	1.07	1.16
ZLS-16	3.73	24.59	6.59	1.36	1.00	1.59	L-M	1.49	0.82	0.96	1.20
ZLS-17	4.16	28.08	6.74	1.31	0.95	1.56	L-M	1.50	0.92	1.22	1.23
ZLS-18	3.02	19.77	6.55	0.90	0.76	1.41	M-H	0.95	0.95	1.25	1.15
ZLS-19	2.22	15.71	7.09	0.64	0.59	1.33	M-H	0.73	0.92	1.33	1.20
ZLS-P	2.01	16.42	8.16	0.70	0.69	1.28	M-H	1.04	0.91	1.25	1.19
ZLS-20	1.86	14.20	7.64	0.60	0.61	1.27	M-H	0.67	0.93	1.25	1.20
ZLS-21	2.22	27.51	12.37	1.35	0.76	2.15	L-M	2.43	1.12	0.43	1.05
Av.1	3.02	19.11	6.46	0.85	0.85	1.23	-	1.01	0.96	1.00	1.15
Av.2	3.95	25.92	7.09	1.06	0.73	1.49	-	1.39	0.90	1.23	1.19

Notes: Av.1, average concentration of coal samples in the K1a coal; Av.2, average concentration of roof and parting. N, REY in coals normalized to Upper continental Crust (UCC); $Ce_N/Ce_N^* = Ce_N/(0.5\times La_N + 0.5\times Pr_N)$; $Eu_N/Eu_N^* = Eu_N/(0.67\times Sm_N + 0.33\times Tb_N)$; $Gd_N/Gd_N^* = Gd_N/(0.33\times Sm_N + 0.67\times Tb_N)$.

shown in Table 3. The Ce anomaly values range from 0.82 to 1.22, with an average of 0.96 in the K1a coal, reflecting weakly negative or no distinct Ce anomalies. The Eu anomaly values are close to 1, indicating that the K1a coal is characterized by a weak Eu anomaly, with the exception of ZLS-10, ZLS-19, and ZLS-21. The samples, ZLS-2 to ZLS-9, ZLS-11 to ZLS-13, and ZLS-16 have weakly negative Eu anomalies. Gd_N/Gd_N^* reflects the weakly positive Gd anomalies in the K1a coal, with values varying from 1.05 to 1.31 (1.15 on average).

5 Discussion

5.1 Sediment source regions

Rare earth elements usually occur in a positive trivalent state (e.g., La^{3+}, Ce^{3+}, etc.), among which the valence states of Ce, Eu, Tb, and Yb can be changed. Under the highly oxidizing, alkaline, and stable water field of the shallow crustal environment, Ce can be converted from trivalent Ce^{3+} to tetravalent state Ce^{4+} (Ce^{4+} has stable Xe electron configuration, $1s^22s^22p^63s^23p^63d^{10}4s^24p^64d^{10}5s^25p^6$) (Elderfield and Greaves, 1981; Braun et al., 1990; Seto and Akagi, 2008; Dai et al., 2016a). Moreover, Eu^{3+} can be reduced to divalent Eu^{2+} under extremely reducing and high-temperature conditions (Sverjensky, 1984; Elderfield, 1988; Bau, 1991). Eu^{2+} is separated from REY^{3+}, because of their difference in alkalinity, resulting in an Eu anomaly relative to the other REY. Thus, the values of Ce_N to Ce_N^* and Eu_N to Eu_N^* are commonly used to reveal the redox decoupling of Ce and Eu from other rare earth elements, and reflect the geochemical composition of the sediment source region (Dai et al., 2016a).

Cerium shows no anomalies in sediment source regions dominated by basaltic lavas or other terrigenous materials (Xiao et al., 2004). In addition, Ce has weak anomalies

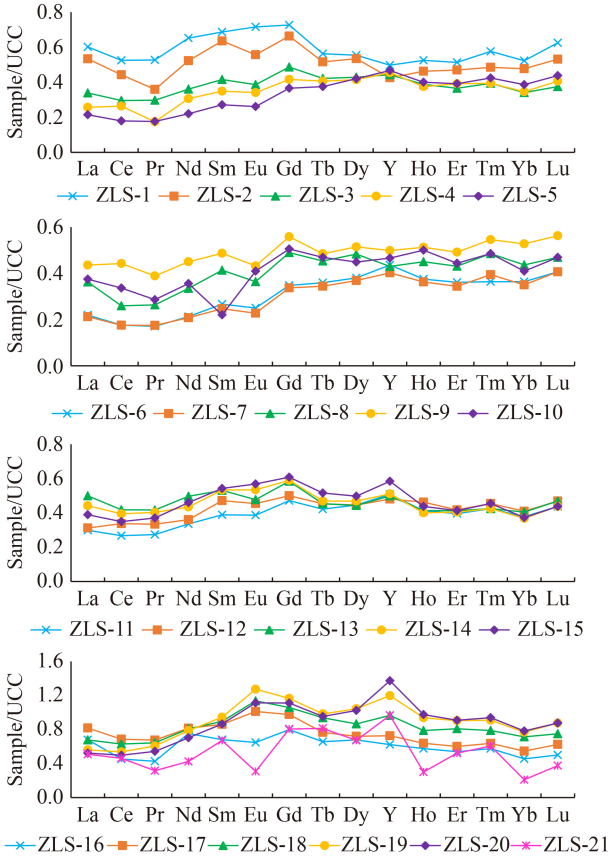

Fig. 7 Distribution patterns of REY in the ZLS K1a coal (UCC values are those of Taylor and McLennan, 1985).

when the sediment source primarily consists of felsic or felsic-intermediate terrigenous rocks (Dai et al., 2016a). The ratios of Ce_N to Ce_N* exhibited weakly negative or no distinct anomalies (av. 0.96), revealing that the felsic or felsic-intermediate rocks terrigenous sediment source for the Zhongliangshan K1a coal.

A Ba/Eu value greater than 1000 in the coal or sedimentary rocks was proposed to judge the interference of Ba on Eu (Yan et al., 2018). If the value of Ba/Eu is > 1000, Ba has significant interference with Eu. The ratios of Ba to Eu in the K1a coal were all lower than 1000 (on average 108, Fig. 8(a)), indicating that the interference of Ba to Eu can be ignored. Europium generally displays negative anomalies in coals with the felsic or felsic-intermediate terrigenous material input, in particular, Eu has a positive anomaly inherited from mafic sediment source regions (Dai et al., 2018; Duan et al., 2019), or input terrigenous materials under high-temperature hydrothermal fluids and a reducing environment (Dai et al., 2016a, 2017). The values of Eu_N/Eu_N* decreased from bottom to top of the seam profile, and the sulfur contents were higher in the bottom of the coal seam, deducing that the coal seam was influenced by hydrothermal fluids in ambient seawater during the early peat accumulation stage (Bau, 1991).

The Gd anomaly can be used to quantify the decoupling of Gd from the other REY. Gadolinium usually exhibits positive, weakly positive or no anomalies. The Gd anomaly is primarily affected by seawater intrusion, hydrothermal fluids, etc., which leads to a positive Gd anomaly (Dai et al., 2016a). The Gd_N/Gd_N* reflects the weak positive Gd anomalies in the K1a coal, with values ranging from 1.05 to 1.31 (1.15 on average), indicating that the coal seam was probably affected by seawater.

The Al_2O_3 to TiO_2 ratio can also be used as a source indicator for sedimentary rocks (Dai et al., 2017; Qin et al., 2018a, 2018b). The Al_2O_3/TiO_2 values of 3–8, 8–21, and 21–70 represent that the sediments were derived from mafic, intermediate, and felsic igneous rocks, respectively (Fig. 8(b)). The values of Al_2O_3/TiO_2 range from 11.25 to 32.29 for the K1a coal, reflecting that the sediment source was derived from felsic-intermediate terrigenous rocks. The Emeishan mantle plume provided terrigenous input for the Late Permian coals in southwestern China, which contained flood basalts, and mafic and felsic intrusions during the same period (Chung and Jahn, 1995; Xiao et al., 2004; Dai et al., 2017). The top of the Emeishan basalt sequence was characterized by felsic-intermediate rocks, which were input as terrigenous sources during peat accumulation (Dai et al., 2017). Combining the anomalies for Ce, Eu, and Gd, and Al_2O_3/TiO_2 of the K1a coal, the sediment source of the K1a coal was dominated

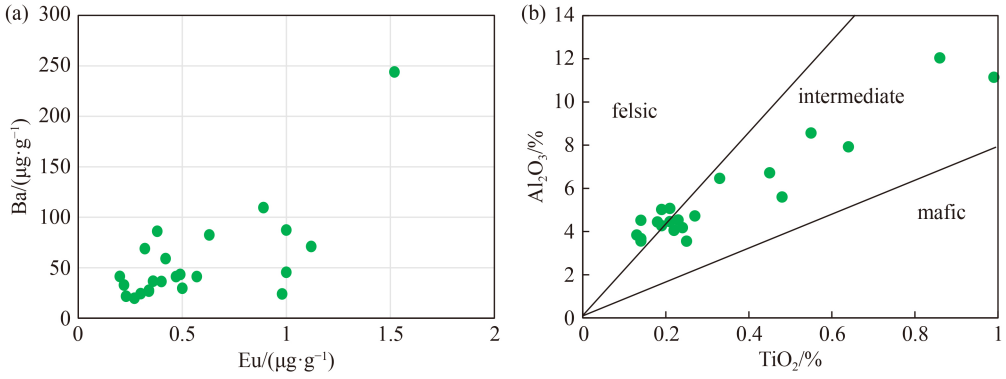

Fig. 8 Diagram of Ba vs. Eu (a), and Al_2O_3 vs. TiO_2 (b) of the K1a coal.

by the felsic-intermediate terrigenous rocks at the top of the Emeishan basalt sequence, and also likely suffered marine intrusion.

5.2 Modes of occurrence of REY

The modes of occurrence of elements are essential for studying the law of elemental migration and combination, formation conditions of ore deposits, and industrial evaluation of ore deposits. Determining the modes of occurrence of valuable elements in coal can provide a scientific basis for their potential as a resource. REY in coal samples commonly occurs in syngenetic detrital and pyroclastic minerals (i.e., zircon, monazite, apatite, and xenotime), and authigenic minerals (aluminum-phosphate-sulfate (APS) minerals, oxides, carbonates, and fluorocarbonates), or associated with the organic matter in coals (Dai et al., 2020, 2021). The modes of occurrence of REY in the K1a coals were investigated using correlation analysis. The correlation analysis of the K1a coals were conducted using SPSS at the 95% confidence level, with the sample number n = 21 and the critical value of correlation coefficient r = 0.433.

The correlations between REY and ash yield, total sulfur, forms of sulfur, and several major element oxides (SiO_2, Al_2O_3, Fe_2O_3, CaO, P_2O_5, etc.) are shown in Fig. 9.

The correlation coefficient between REY and ash yield in the Zhongliangshan coals is 0.65 (Fig. 9(a)), indicating that REY mainly occur in the inorganic component. Moreover, REY are significantly correlated with SiO_2 (0.63), Al_2O_3 (0.68), SiO_2 + Al_2O_3 (0.66), and P_2O_5 (0.65), (Figs. 9(b)–9(e)), reflecting that REY possibly occur in aluminosilicate and phosphate minerals or arise from the same solutions or origins (Dai et al., 2020, 2021). The minerals in coal are mainly kaolinite and illite based on the XRD analysis, thus, REY are speculated to occur in aluminosilicate minerals, which is consistent with the terrigenous detrital sediment resource. The rare earth elements and yttrium can be released from the mineral crystal lattice by breaking the stable Si-Al bond, providing theoretical support for achieving a high extraction yield. The correlation between REY and ash and its main component SiO_2 + Al_2O_3, is consistent with the results of Qin et al. (2018a) and Duan et al. (2019). In addition, REY are closely related to SiO_2, Al_2O_3, and SiO_2 + Al_2O_3, however, the quartz content in coals is low, revealing that quartz cannot be the main REY carrier (Tang and Huang, 2004). Although the correlation coefficient of REY with total sulfur, inorganic sulfur, and Fe_2O_3 are high (Figs. 9(f)–(h)), and the correlation between REY and organic sulfur is low (0.41), however, Dai et al. (2021) reported that REY cannot occurs in sulphide minerals, conjecting that REY are related to the inorganic component, and it may be influenced by the marine intrusion. REY are negatively correlated with CaO (Fig. 9(i)), indicating that the REY are not associated with calcite. Moreover, REY are positively correlated with Zr (Fig. 9(j)), because they are adjacent on the periodic table and are more likely to be substituted into the zircon lattice (Li et al., 2020b).

Furthermore, correlation analysis were conducted for LREY, MREY, and HREY with the ash yield, SiO_2, Al_2O_3, SiO_2 + Al_2O_3, Fe_2O_3, total sulfur, CaO, P_2O_5, and Zr (Fig. 10). The results showed that LREY, MREY, and HREY are negatively correlation with CaO, but positively correlated with other parameters. Specifically, the correlation coefficients of LREY with the ash yield, SiO_2, Al_2O_3, SiO_2 + Al_2O_3, Fe_2O_3, P_2O_5, and Zr are higher than those of HREY and MREY, indicating that LREY preferentially substitutes into the crystal lattice of minerals, such as aluminosilicate, phosphate, and zircon. The correlations of LREY, MREY, and HREY with sulfur are the same as those of REY with sulfur in the Zhongliangshan coal. The correlation of HREY-S is higher than LREY-S and MREY-S, reflecting that HREY are more susceptible to seawater intrusion. The negative correlations of LREY-CaO, MREY-CaO, and HREY-CaO are consistent with those of REY-CaO, and each rare earth element cannot exist in the calcium-containing minerals.

5.3 Evaluation of REY in the K1a coal

The average concentrations of each rare earth element and yttrium within the average world coal were estimated by Ketris and Yudovich (2009), and the total REY concentration is 68.5 μg/g. The average REY concentration of world coal ash (404 μg/g, Ketris and Yudovich, 2009) is approximately 6 times higher than that of world coal. REY oxides (REO) are commonly used to assess the abundance of these elements in deposits. Corresponding to the REY content of world coal, the REO concentration is 483 μg/g. For Chinese coals, the average REY concentration reaches 138 μg/g, which is higher than that of world coal (Dai et al., 2012b). Hence, the REY in Chinese coal or coal ash may have a higher availability and economic value.

To evaluate rare earth elements and yttrium as promising alternative sources in coal or coal by-products, many factors must considered, such as coal mining capacity, REY resources, possibility of beneficiation, extraction yield, supply-demand relationship, environment, and human health issues (Seredin and Dai, 2012; Dai et al., 2017). Nevertheless, the REY grade and elemental composition can provide an initial assessment of the REY prospect. The first criterion is REO, whose concentration is greater than 1000 μg/g in coal ash, which can be considered as the cut-off grade for beneficial recovery (Seredin and Dai, 2012). The second criterion is the outlook coefficient (C_{outl}), which is the ratio of the relative amount of critical REY (Nd, Eu, Tb, Dy, Er, Y) in the total REY to the relative amount of excessive REY

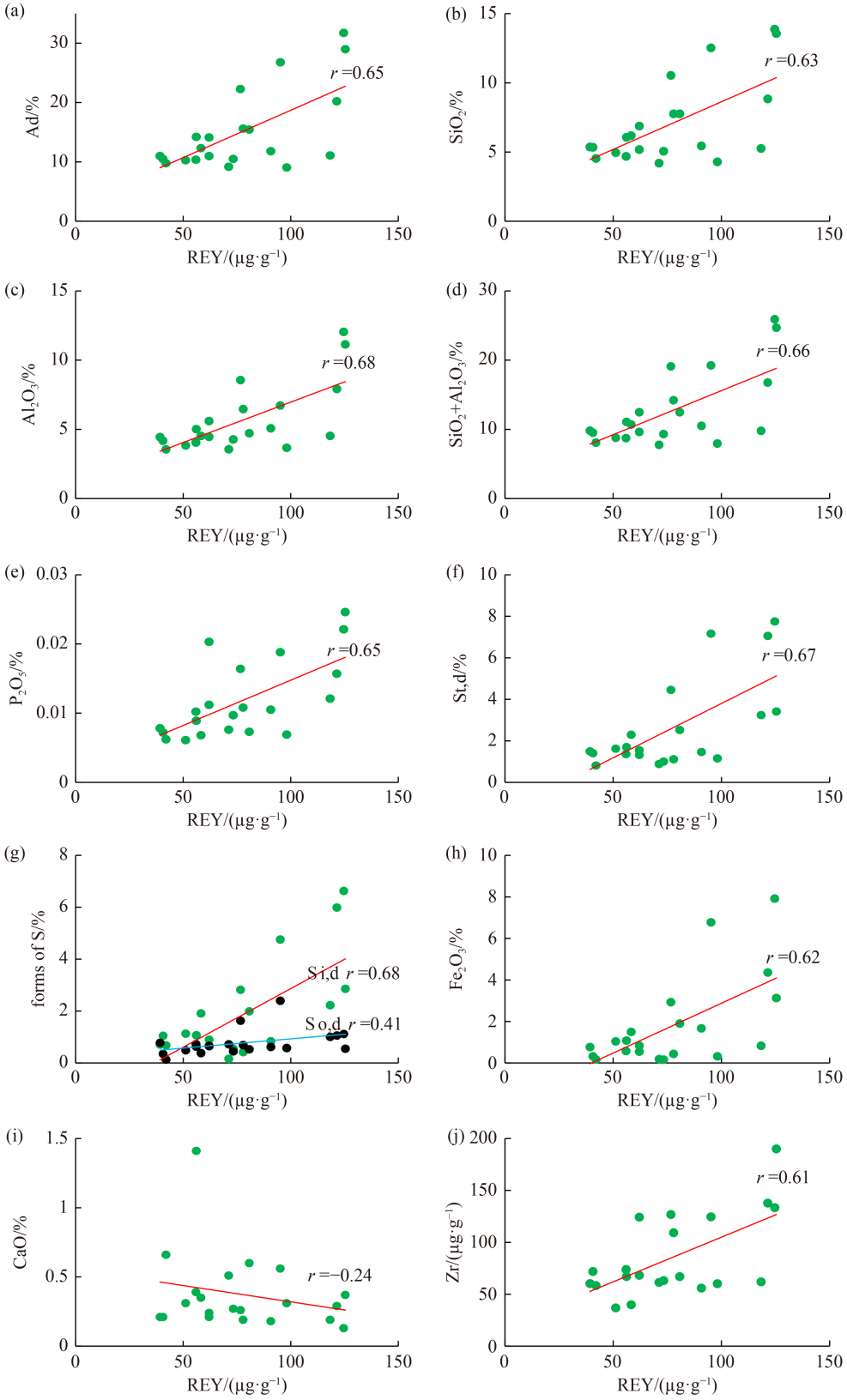

Fig. 9 Correlation between REY and A_d, SiO_2, Al_2O_3, $SiO_2 + Al_2O_3$, P_2O_5, $S_{t,d}$, $S_{i,d}$, $S_{o,d}$, Fe_2O_3, CaO, and Zr.

(Ce, Ho, Tm, Yb, Lu) (Eq. (1)). As REY are non-volatile elements, their relative enrichment index (REI) from coal to ash is assumed to be 1. The REY content in coal can be converted to that in ash through the ash yield (Eq. (2)).

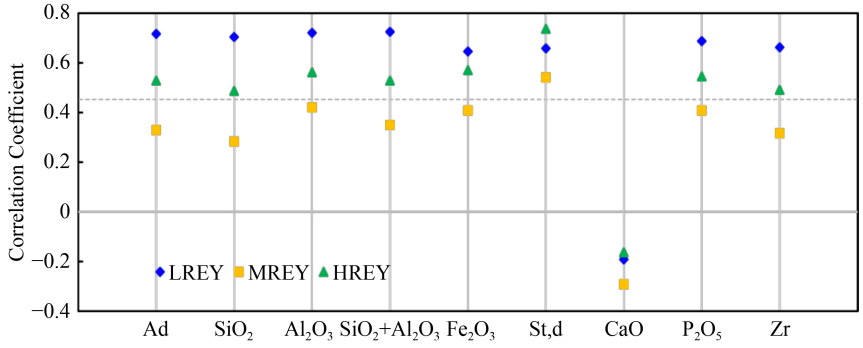

Fig. 10 Correlation between LREY, MREY, HREY with A_d, SiO_2, Al_2O_3, $SiO_2 + Al_2O_3$, Fe_2O_3, $S_{t,d}$, CaO, P_2O_5, and Zr.

Then, according to the law of conservation of mass, the concentrations of REO in the ash were calculated using Eqs. (3):

$$C_{\text{outl}} = \frac{(\text{Nd}+\text{Eu}+\text{Tb}+\text{Dy}+\text{Er}+\text{Y})/\sum\text{REY}}{(\text{Ce}+\text{Ho}+\text{Tm}+\text{Yb}+\text{Lu})/\sum\text{REY}}, \quad (1)$$

$$C_{\text{ash}-R} = \frac{\text{C}_{\text{coal}-R}}{A_{\text{d}}} \times REI, \quad (2)$$

$$C_{\text{ash}-\text{R}_2\text{O}_3} = \frac{\text{C}_{\text{ash}-\text{R}} \times \text{M}_{\text{R}_2\text{O}_3}}{2 \times M_R}, \quad (3)$$

where A_d, ash yield; *REI,* relative enrichment index; *R*, single rare earth elements; *M*, molar mass; $C_{\text{coal-}R}$, *R* concentration in coal; $C_{\text{ash-}R}$, *R* concentration in ash; and $C_{\text{ash}-\text{R}_2\text{O}_3}$, R_2O_3 concentration in ash.

The source of REY with $C_{\text{outl}} > 2.4$ and $0.7 \leqslant C_{\text{outl}} \leqslant 1.9$ are considered to be highly promising and promising REY raw materials, respectively. Combining these two criteria, the total REY oxides (REO) vs. outlook coefficient (C_{outl}) of the K1a coal was drawn in Fig. 11. According to the relationship between REO and C_{outl}, most coal samples fell within the unpromising area. In particular, the ZLS-16 and ZLS-20 have higher outlook coefficients (1.23 and 1.59) and REO concentrations (1278.49 μg/g and 1273.06 μg/g), which fall within the promising area. The average outlook coefficient and REO concentration of the K1a coal are 1.15 and 656.34 μg/g, respectively, and these fall within the unpromising area. Since the roof and parting have a high ash yield, the REO in ash are low, with 332.21 μg/g and 227.46 μg/g. Overall, the combustion products of the K1a coal seam have no potential economic value and are not suitable as REY raw materials, except for the ZLS-16 and ZLS-20 samples.

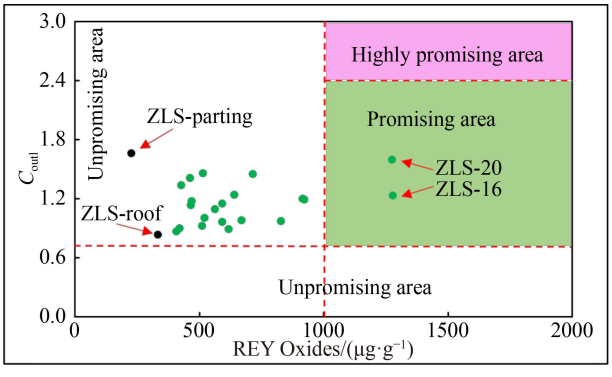

Fig. 11 Evaluation of REY in ZLS K1a coal ash (roof and parting are presented by black point).

5.4 Evaluation of REY in coal deposits from southwestern China

Currently, coal is primarily used for thermal power generation in China. The utilization value of coal ash is low (restricted to usee in building materials) and its accumulation results in occupation of land resources, and the migration of hazardous elements is harmful to the environment and human health. Additionally, rich coal reserves exist in southwestern China, such as those in Guizhou, Yunnan, Sichuan, and Chongqing. Therefore, it is significant to explore high-value utilization of coal ash and reduce its harmful effects.

In this study, the abundance and distribution area of REY in Permian coals from coal deposits in southwest China were ascertained, to reveal the potential of REY in coal ash as an alternative resource (Table 4). The average REY concentration for the entire coal mine or seam was calculated based on the weighted average of the thickness and the REY concentration. The concentration contours of REY based on the REY content in coals from the investigated coalfields or coal mines were drawn in Fig. 12. The concentrations of REY in coals from the Yudai and Jinqi mines of the Qiandongbei coalfield are highest, reaching 636.7 μg/g and 678.6 μg/g, respectively. The detrital materials of the Qiandongbei coalfield were derived from the mixing of felsic volcanic ash resembling a peralkaline rhyolite composition and Emeishan Large Igneous Province (ELIP) basaltic eroded products (Li et al., 2020b). High REY also exist in coals from the Dahebian mine, Shiping mine, Lvshuidong mine, and the Tianfu coalfield, with weighted average contents of more than or approximately 300 μg/g. Elevated concentrations

Table 4 REY concentration (μg/g) and some parameters of coals from southwestern China

Region	coalfield	Mine	Seam	Age	T	A_d	La	Ce	Pr	Nd	Sm	Eu	Gd	Tb	Dy	Y	Ho	Er	Tm	Yb	Lu	REY	REO	Coutl	Ref.
Chongqing	ZLS	ZLS	K1a	P_2l	2.1	15.1	13.22	24.76	2.64	12.38	2.44	0.5	2.45	0.36	1.97	13.57	0.41	1.15	0.17	1	0.16	77.2	607.4	1.13	This paper
Chongqing	ZLS	ZLS	K1a	P_2l	1.2	18.7	17	36	4	17	0.6	0.1	0.3	0.1	0.1	12	0.6	1.4	0.1	1.2	0.1	90.6	572.9	0.81	Zhuang et al., 2005
Chongqing	ZLS	ZLS	K1b	P_2l	2	29.6	25	54	7	29	2.2	0.1	2.5	0.1	2.4	21	0.9	2.3	0.2	2.2	0.2	149.1	595.6	0.95	
Chongqing	TF	MXP	K2	P_2l	3.1	14.5	49.12	72.45	9.93	32.48	5.67	0.6	5.75	1.03	4.3	33.83	1.18	2.54	0.49	2.27	0.48	222.1	1810.6	0.97	Qin et al., 2018a
Chongqing	TF	MXP	K2	P_2l	0.4	12.1	52.1	95.1	10.7	40.9	6.96	0.87	9.01	1.34	8.26	46.1	1.68	5.13	0.72	4.83	0.69	284.4	2777.6	1.00	Dai et al., 2017
Chongqing	TF	MXP	K1	P_2l	0.4	41.5	62.3	107	16.5	71.1	14.9	3.45	16.6	2.35	14	95.3	2.74	7.9	1.04	6.68	0.97	422.8	1210.7	1.64	
Chongqing	TF	MXP	K2	P_2l	4	27.2	91	177	20	85	11	0.3	12	0.1	9.5	53	2.2	6.4	0.9	6.6	0.8	475.8	2063.0	0.82	Zhuang et al., 2005
Chongqing	TF	MXP	K4	P_2l	0.5	22.6	50	113	13	48	5.4	0.1	4.7	0.1	4.8	32	1.5	3.6	0.5	4.1	0.3	281.1	1467.6	0.74	
Chongqing	TF	MXP	K5	P_2l	0.6	25.2	29	65	7	31	2.3	0.1	3.4	0.1	3.7	32	1.4	3	0.7	3.4	0.4	182.5	858.6	0.99	
Chongqing	TF	MXP	K7	P_2l	0.6	40.0	34	77	9	43	4	0.1	2.8	0.1	2.1	17	0.9	2.1	0.2	2.5	0.3	195.1	574.2	0.80	
Chongqing	NT	DL	4	P_2l	2.03	13.5	17.8	34.8	3.9	15	2.99	0.55	3.3	0.46	2.7	13.4	0.52	1.53	0.21	1.44	0.2	98.8	867.0	0.91	Chen et al., 2015
Chongqing	NT	DL	6	P_2l	0.72	10.9	19.9	39.3	4.43	16.8	3.32	0.42	3.78	0.56	3.51	18.4	0.7	2.08	0.28	1.94	0.28	115.7	1253.8	0.98	
Chongqing	SZ	-	12	P_2l	0.48	69.18	174.8	18.37	72.48	12.97	1.96	11.71	1.754	10.86	68.34	2.34	7.43	0.988	6.63	0.99	460.8	69.18	1548.2	0.88	Dai et al., 2010b
Chongqing	SZ	-	11	P_2l	0.24	33.2	71.5	137	16.2	58.5	10.6	1.32	8.77	1.32	7.9	42.1	1.6	4.95	0.67	4.49	0.66	367.6	1305.7	0.80	
Chongqing	SZ	-	10	P_2l	0.36	31.9	58.3	108	13.6	51.2	10.3	1.74	8.94	1.3	7.55	38.8	1.55	4.86	0.66	4.42	0.65	311.9	1154.2	0.91	
Chongqing	SZ	-	9	P_2l	0.41	34.2	14.3	28	3.38	12.9	2.72	0.5	2.81	0.5	3.13	18.8	0.67	2.12	0.3	2.02	0.31	92.5	321.2	1.21	
Chongqing	SZ	-	8	P_2l	1.83	15.5	26.2	49.3	5.8	21.3	4.18	0.75	3.71	0.59	3.6	18.8	0.73	2.21	0.3	1.98	0.29	139.7	1067.7	0.90	
Chongqing	SZ	-	7	P_2l	0.51	26.0	28.1	51.3	6.1	23.5	4.72	1.11	4.17	0.6	3.6	19.2	0.72	2.25	0.29	2.01	0.3	148.0	672.3	0.92	
Chongqing	SZ	-	6	P_2l	1.16	25.7	12.9	25	3.09	12.2	2.57	0.61	2.53	0.4	2.59	14.4	0.53	1.69	0.23	1.59	0.24	80.6	371.2	1.16	
Chongqing	SECQ	DG	K1	P_2wjp	0.85	24.5	26	48.6	7.27	31.1	6.96	1.55	8.56	1.3	8.12	61.4	1.68	5.04	0.66	4.25	0.63	213.1	1038.8	1.94	Zou et al., 2020
Guizhou	QDB	YD	4	P_2wjp	1	24.2	116.3	241.2	24.32	88.95	18.49	1.417	16.51	2.395	15.79	86.75	3.26	9.17	1.324	9.535	1.358	636.7	3105.0	0.80	Li et al., 2020b
Guizhou	QDB	JQ	4	P_2wjp	1.18	25.2	122	242	24.59	88.15	18.87	1.541	17.83	2.698	19.32	113.5	3.841	10.9	1.538	10.37	1.418	678.6	3186.2	0.91	
Guizhou	LPS	TC	3	P_2l	1.62	14.7	11.1	23.3	2.62	10.6	2.16	0.38	2.26	0.31	1.86	10.4	0.38	1.12	0.15	1.04	0.16	67.8	546.6	0.99	Liu et al., 2020
Guizhou	LPS	TC	6	P_2l	1.45	20.4	14.2	30.9	3.62	15.3	3.36	0.67	3.67	0.54	3.39	18.6	0.69	2.02	0.28	1.911	0.28	99.4	578.7	1.19	

(*Continued*)

Region	coalfield	Mine	Seam	Age	T	A_d	La	Ce	Pr	Nd	Sm	Eu	Gd	Tb	Dy	Y	Ho	Er	Tm	Yb	Lu	REY	REO	Coutl	Ref.
Guizhou	LPS	DHB	D101	P_2l	0.89	18.0	73.3	158	18.8	72	13.2	2.05	13	1.6	8.96	42	1.65	4.9	0.68	4.61	0.66	415.4	2715.9	0.79	Liu et al., 2019
Guizhou	LPS	WJZ	w407	P_2l	1.2	14.4	28.6	70.8	8.08	33.3	6.5	1.47	13	1.6	3.6	16.4	0.65	1.81	0.24	1.65	0.24	187.9	1537.1	0.79	
Guizhou	LPS	YLT	19	P_2l	1.7	22.8	16.11	35.09	3.889	15.22	3.098	0.667	3.378	0.504	3.148	14.34	0.606	1.825	0.25	1.695	0.237	100.1	517.5	0.94	Wang et al., 2016
Guizhou	TZ	CLB	4	P_2wjp	2.25	15.2	22.12	40.93	4.278	16.14	3.104	0.129	2.68	0.152	1.918	12.36	0.137	1.196	0	1.184	0	106.3	824.0	0.75	Li et al., 2019
Guizhou	ZN	FHS	23	P_2l	3.29	12.2	13.58	28.27	3.14	10.76	2.31	0.77	2.28	-	1.92	9.99	-	0.96	-	-	-	74.8	836.8	0.86	Li et al., 2017
Guizhou	ZN	FHS	27	P_2l	1.26	23.8	13.97	28.70	3.30	10.89	2.17	0.67	2.18	-	2.20	12.81	-	1.41	-	1.32	-	79.6	766.0	0.93	
Guizhou	ZN	WJB	6	P_2wjz	1.88	17.7	11.31	23.48	2.69	9.11	2.03	0.65	1.96	-	1.90	10.01	-	1.12	-	-	-	65.2	624.6	0.97	
Guizhou	ZN	WJB	7	P_2wjz	1.05	29.7	13.57	28.71	3.27	11.08	2.22	0.70	2.19	-	2.20	10.57	-	1.18	-	1.10	-	76.9	382.0	0.86	
Guizhou	ZN	KLS	6	P_2l	1.35	14.9	16.50	34.90	4.23	17.20	3.28	0.67	3.33	0.44	2.54	12.20	0.48	1.33	0.18	1.21	0.17	98.7	782.4	0.93	Liu et al., 2021
Guizhou	ZN	SJC	7	P_2l	1.75	16.6	14.40	29.80	3.27	12.70	2.52	0.44	2.72	0.40	2.50	12.70	0.50	1.45	0.20	1.34	0.19	85.1	608.2	0.94	
Guizhou	GD	GC	3	P_2wjp	1.01	17.7	6.48	13.6	1.59	6.73	1.4	0.3	1.65	0.25	1.8	15.4	0.39	1.3	0.18	1.29	0.22	52.6	355.3	1.64	Dai et al., 2015b
Guizhou	GD	HST	3	P_2wjp	1.03	29.7	13.8	29.6	3.24	13.3	2.43	0.55	2.59	0.35	2.19	14	0.43	1.35	0.18	1.28	0.21	85.5	340.9	1.00	
Yunnan	ZX	RSH	C_5b	P_2l	1.75	29.9	18.01	37.85	5.066	20.71	4.183	0.851	4.277	0.597	3.16	13.91	0.626	1.817	0.277	1.854	0.289	113.5	447.1	1.00	Duan, 2017
Yunnan	XW	BL	C1	P_2xw	1.46	28.7	30.7	67.9	7.54	29	5.85	1.08	6.18	0.88	3.93	20.8	0.77	2.05	0.29	1.94	0.3	179.2	736.3	0.81	Li et al., 2021
Yunnan	XW	LB	C1	P_2xw	2.35	34.5	21.95	49.36	5.548	21.81	4.423	0.864	4.748	0.737	3.655	20.13	0.746	2.055	0.287	1.897	0.291	138.5	474.9	0.94	
Sichuan	GX	SP	19	P_2l	0.50	17.4	5.48	11.7	1.29	4.72	1.08	0.254	1.34	0.222	1.39	10.6	0.313	0.969	0.149	0.994	0.159	40.7	278.4	1.36	Luo et al., 2016
Sichuan	GX	SP	25	P_2l	1.30	27.3	77.86	143.5	18.6	69.1	13.28	1.347	14.16	2.16	12.74	87.25	2.672	7.771	1.111	7.149	1.048	459.7	1995.1	1.16	
Sichuan	GX	SP	25	P_2l	1.10	21.0	51.47	90.13	10.76	41.33	7.809	0.811	8.636	1.229	7.288	46.15	1.437	4.329	0.585	3.864	0.548	276.4	1562.6	1.05	Dai et al., 2016b
Sichuan	HYS	LSD	K1	P_2l	2.03	20.9	51.5	105	12.4	46.8	8.61	1.06	8.94	1.33	7.46	41.8	1.54	4.48	0.67	4.41	0.67	296.7	1680.0	0.92	Dai et al., 2014b

Notes: T, thickness (m); A_d, ash (%); Ref., references; P_2l, Late Permian Longtan Formation; P_2wjp, Late Permian Wujiaping Formation; P_2wjz, Late Permian Wangjiazhai Formation; P_2xw, Late Permian Xuanwei Formation; ZLS, Zhongliangshan; TF, Tianfu; MXP, Moxinpo; NT, Nantong; DL, Donglin; SZ, Songzao; TH, Tonghua; YY, Yuyang; FC, Fengchun; SH, Shihao; SECQ, Southeastern Chongqing; DG, Donggou; QDB, Qiandongbei; YD, Yudai; JQ, Jinqi; LPS, Liupanshui; TC, Tucheng; DHB, Dahebian; WJZ, Wangjiazhai; YLT, Yueliangtian; TZ, Tongzhi; CLB, Chailinbao; ZN, Zhina; FHS, Fenghuangshan; WJB, Wenjiaba; KLS, Kulishu; SJC, Sijichun; GD, Guiding; GC, Guanchong; HST, Heishentian; ZX, Zhengxiong; RSH, Reshuihe; XW, Xuanwei; BL, Bole; LB, Laibin; GX, Guxu; SP, Shiping; HYS, Huayingshan; LSD, Lvshuidong.

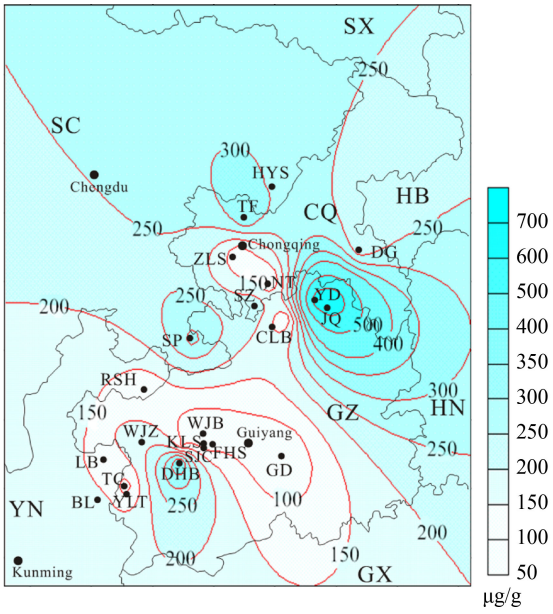

Fig. 12 The content contour image of total REY in coals from southwestern China.

of REY in the D101 coal of the Dahebian mine were derived from alkaline volcanic materials on the top of the ELIP sequence (terrigenous input) and from airborne volcanic ash (tonstein parting) (Liu et al., 2019). The detrital sources of the No. 25 coal from the Shiping mine in the Guxu coalfield and the Moxinpo mine in the Tianfu coalfield were felsic-intermediate terrigenous rocks at the top of the Emeishan basalt sequence, and there was hydrothermal solution input into the No. 25 coal during early peat accumulation (Dai et al., 2016a, 2017). The REY concentration of 90.6 μg/g in the K1a coal from the Zhongliangshan coalfield reported by Zhuang et al. (2007) is close to that in this study. The REY are slightly enriched in the Reshuihe coal mine of the Zhenxiong coalfield, and the Bole and Laibin coal mines of the Xuanwei coalfield in Yunnan Province. However, the REY contents in western and central Guizhou are low, including the Liupanshui coalfield (Tucheng and Yueliangtian), Zhina coalfield (Kulishu, Sijichun, Fenghuangshan, and Wenjiaba), and Guiding coalfield (Guanchong and Heishentian). The Tucheng coal was derived mostly from distal volcanic arcs and orogens, and high-Ti Emeishan basalts (Liu et al., 2019). The terrigenous materials of the Kulishu and Sijichun coals were mixture of the Emeishan volcanics and the less abundant Neoproterozoic metamorphic-granite complex (Liu et al., 2021). The supply of terrigenous materials, input of felsic-alkaline volcanic ash, intrusion of seawater, and injection of hydrothermal fluids are the dominant factors affecting the inorganic components in coals (Liu et al., 2021).

The outlook coefficients of all collected samples show that the coal or coal by-products can be considered REY raw materials because the relative proportion of critical to excessive REY in coal is > 0.7 (Fig. 13). Combined with the concentration of REO in coal ash, the results reflect that the Qiandongbei coalfield (QDB), Dahebian (Liupanshui coalfield, LPS-DHB), Lvshuidong (Huayingshan coalfield, HYS-LSD), Shiping (Guxu coalfield, GX-SP), Moxinpo (Tianfu coalfield, TF-MXP), Wangjiazhai (Liupanshui coalfield, LPS-WJZ), Songzao coalfield (SZ), and Donggou (Southeastern Chongqing coalfield, SECQ-DG) coals are suitable as potential REY sources. In addition, the Donglin (Nantong coalfield, NT-DL), Chalinbao (Tongzhi coalfield, TZ-CLB), Fenghuangshan (Zhina coalfield, ZN-FHS), and Kulishu (Zhina coalfield, ZN-KLS) coals can be selected as reserve REY sources, owing to the worldwide increase in prices and demand for REY.

5.5 REY extraction suggestions

Coal combustion products enriched with REY have a higher recovery potential. As reported in the literature, aluminosilicates (glass phase and mullite) in fly ash, bottom ash, and slag from the Chongqing Power Plant account for 75.5%, 69.1%, and 89.8%, respectively (Xu et al., 2022). REY occurrences in coal ash are dominated by an aluminosilicate glass phase (Si-Al), discrete minerals phase (i.e., mullite, quartz), and organic matter, in which the REY exist in the aluminosilicate glass phase are more easily leached than the minerals phase (Fu et al., 2022; Xu et al., 2022). Therefore, to improve the leaching efficiency of REY in coal ash, it is crucial to break the Si-Al bond and release REY wrapped in the glass phase and mineral lattice.

The extraction processes of coal ash primarily include activation pretreatment, leaching, separation and impurity removal. Because of the complex composition of coal-burning products, there is no fixed technology for extracting REY from coal ash. The pretreatment of ash

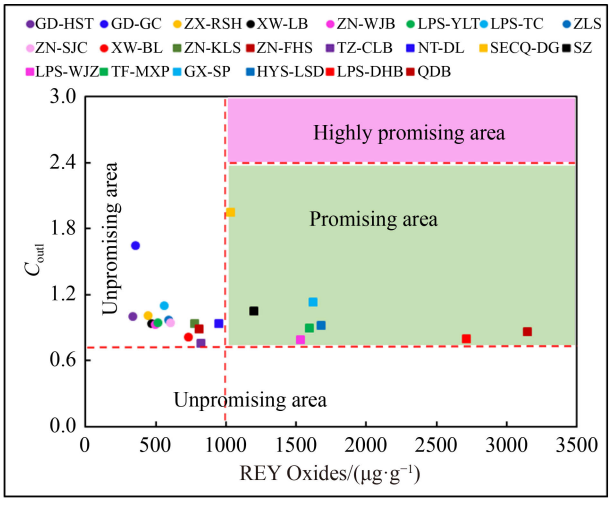

Fig. 13 Diagram of the REO vs. C_{outl} from some coalfields of southwestern China.

uses cooperative mechanical and chemical activation to increase the activity of coal ash, and improve the subsequent leaching yield of REY. The mechanical activation of coal ash involves sorting or grinding to initially enrich the REY or destroy the surface glassy Si-Al bond. Chemical activation refers to the alkali reagent (Na_2CO_3, Na_2O_2, NaOH, etc.), which is molten at high temperatures and reacts with coal ash, to destroy the silicon aluminum structure of coal ash and convert the insoluble mineral phases into soluble aluminosilicates (i.e., sodium silicate and sodium aluminosilicate) (Taggart et al., 2018). Taggart et al. (2018) reported that the leaching yield of coal ash mixed with Na_2O_2 and NaOH is better than that of Na_2CO_3 under the same conditions, and the melting point of Na_2CO_3 is higher than those of the other two alkalis. The alkali roasting of NaOH and Na_2CO_3 process significantly enhanced the REY leaching yields to 79% and 89%, respectively, compared with 20% REY in baseline acid leaching (Pan et al., 2021). Acid, acid-base combinations, and biological leaching are common leaching methods and are supplemented by microwave, ultrasonic or stirring to improve the leaching yield of REY (Lin et al., 2018; Cao, 2019; Mondal et al., 2019; Wang et al., 2019). Besides, the reagent, time, temperature, solid to liquid ratio, and coal ash itself could also affect the leaching efficiency. Wang et al. (2019) used an acid-base combination (HCl, NaOH) cycle for leaching REY from coal fly ash, and the results showed that this method can effectively remove the mineral phase of active silica (41.10%) and release the contained REY. The optimal extraction yield of REY reaches 88.15%, which is higher than that of single HCl leaching. Separation and purification methods in the laboratory include precipitation, impregnation resin, and membrane separation methods (Mondal et al., 2019; Smith et al., 2019; Zhang and Honaker, 2020). Based on existing studies, using mechanical activation pretreatment to generate concentrates with higher REY content, alkali roasting and acid leaching can enhance the economic viability of the REY extraction. Moreover, REY recovery also must consider the degree of corrosion of the reagents to the reaction equipment, the degree of environmental pollution, and the economy.

6 Conclusions

Rare earth elements and yttrium are considered strategic metals because of their scarcity and changing supply-demand relationships. Coal resources are projected to be an important fuel source for decades. Although REY are trace elements in coal deposits, many basic geochemical research has verified that REY can be enriched in coal and its combustion products, and can be used as an alternative source for REY. Abundant coal resources are concentrated in southwestern China, and contain inorganic elements, particularly REY.

Compared to the average world coal, REY have normal level in the Zhongliangshan K1a coal, and have a high fractionation degree. There are three enrichment types, including M-H-type, L-M-type, and H-type, because the fractionation of MREY and HREY are higher than that of LREY. The dominant sediment source for the K1a coal was felsic-intermediate terrigenous rocks at the top of the Emeishan basalt sequence. Meanwhile, marine waters also influenced the K1a coal seam. REY mainly occurs in aluminosilicates, phosphate minerals or zircon lattices. In Particular, LREY preferentially substitutes into the minerals than MREY and HREY.

Owing to the relatively low content of REY in the coals, the combustion products of the K1a coal have no potential economic value for REY recovery. However, REY are enriched in other coal deposits from southwestern China, primarily concentrated in areas other than central Guizhou, southwestern Chongqing, and the junction of western Guizhou and northeastern Yunnan, and its coal ash can be considered as alternative REY raw materials during shortage periods. The assessment of the economic viability of REY extraction from coal ash is not sufficient. Collaborative extraction of valuable metal elements from coal ash, while considering the principles of economy and environmental issues, is the focus of future research.

Acknowledgments We thank the editor and anonymous reviewers for their comments to improve the manuscript. This research was supported by the National Natural Science Foundation of China (Grant Nos. U1903207, 42172191, 41972176, and 42002184), Natural Science Foundation of Hebei (No. D2021402013), Fundamental research Funds of China University of Mining and Technology (No. 2020CXNL11), and Priority Academic Program Development of Jiangsu Higher Education Institutions.

References

ASTM Standard D2492–02 (2002). Standard Test Method for Forms of Sulfur in Coal. ASTM International, West Conshohocken, PA

ASTM Standard D3173–11 (2011). Standard Test Method for Moisture in the Analysis Sample of Coal and Coke. ASTM International, West Conshohocken, PA

ASTM Standard D3174–11 (2011). Standard Test Method for Ash in the Analysis Sample of Coal and Coke. ASTM International, West Conshohocken, PA

ASTM Standard D3175–11 (2011). Standard Test Method for Volatile Matter in the Analysis Sample of Coal and Coke. ASTM International, West Conshohocken, PA

ASTM Standard D3177–02 (2002). Standard Test Methods for Total Sulfur in the Analysis Sample of Coal and Coke. ASTM International, West Conshohocken, PA

Bau M (1991). Rare-earth element mobility during hydrothermal and metamorphic fluidrock interaction and the significance of the oxidation state of europium. Chem Geol, 93(3–4): 219–230

Bau M, Schmidt K, Koschinsky A, Hein J, Kuhn T, Usui A (2014).

Discriminating between different genetic types of marine ferro-manganese crusts and nodules based on rare earth elements and yttrium. Chem Geol, 381: 1–9

Braun J J, Pagel M, Muller J P, Bilong P, Michard A, Guillet B (1990). Cerium anomalies in lateritic profiles. Geochim Cosmochim Acta, 54(3): 781–795

Cao S S (2019). Research of enhanced leaching of rare earth elements in coal fly ash under low temperature conditions. Dissertation for the Doctoral Degree. Xuzhou: China University of Mining and Technology (in Chinese)

Chen J, Chen P, Yao D X, Liu Z, Wu Y S, Liu W Z, Hu Y B (2015). Mineralogy and geochemistry of Late Permian coals from the Donglin Coal Mine in the Nantong coalfield in Chongqing, southwestern China. Int J Coal Geol, 149: 24–40

Chung S L, Jahn B M (1995). Plume-lithosphere interaction in generation of the Emeishan flood basalts at the Permian – Triassic boundary. Geology, 23(10): 889–892

Dai S F, Graham I T, Ward C R (2016a). A review of anomalous rare earth elements and yttrium in coal. Int J Coal Geol, 159: 82–95

Dai S F, Hower J C, Finkelman R B, Graham I T, French D, Ward C R, Eskenazy G, Wei Q, Zhao L (2020). Organic associations of non-mineral elements in coal: a review. Int J Coal Geol, 218: 103347

Dai S F, Liu J J, Ward C R, Hower J C, French D, Jia S H, Hood M M, Garrison T M (2016b). Mineralogical and geochemical compositions of Late Permian coals and host rocks from the Guxu Coalfield, Sichuan Province, China, with emphasis on enrichment of rare metals. Int J Coal Geol, 166: 71–95

Dai S F, Luo Y B, Seredin V V, Ward C R, Hower J C, Zhao L, Liu S D, Zhao C L, Tian H M, Zou J H (2014b). Revisiting the late Permian coal from the Huayingshan, Sichuan, southwestern China: enrichment and occurrence modes of minerals and trace elements. Int J Coal Geol, 122: 110–128

Dai S F, Ren D Y, Chou C L, Finkelman R B, Seredin V V, Zhou Y P (2012b). Geochemistry of trace elements in Chinese coals: a review of abundances, genetic types, impacts on human health, and industrial utilization. Int J Coal Geol, 94: 3–21

Dai S F, Finkelman R B, French D, Hower J C, Graham I T, Zhao F H (2021). Modes of occurrence of elements in coal: a critical evaluation. Earth Sci Rev, 222: 103815

Dai S F, Seredin V V, Ward C R, Hower J C, Xing Y W, Zhang W G, Song W J, Wang P P (2015b). Enrichment of U-Se-Mo-Re-V in coals preserved within marine carbonate successions: geochemical and mineralogical data from the Late Permian Guiding Coalfield, Guizhou, China. Miner Depos, 50(2): 159–186

Dai S F, Seredin V V, Ward C R, Jiang J H, Hower J C, Song X L, Jiang Y F, Wang X B, Gornostaeva T, Li X, Liu H D, Zhao L X, Zhao C L (2014a). Composition and modes of occurrence of minerals and elements in coal combustion products derived from high-Ge coals. Int J Coal Geol, 121: 79–97

Dai S F, Wang P P, Ward C R, Tang Y G, Song X L, Jiang J H, Hower J C, Li T, Seredin V V, Wagner N J, Jiang Y F, Wang X B, Liu J J (2015a). Elemental and mineralogical anomalies in the coal-hosted Ge ore deposit of Lincang, Yunnan, southwestern China: key role of N_2-CO_2-mixed hydrothermal solutions. Int J Coal Geol, 152: 19–46

Dai S F, Wang X B, Chen W M, Li D H, Chou C L, Zhou Y P, Zhu C S, Li H, Zhu X W, Xing Y W, Zhang W G, Zou J H (2010b). A high-pyrite semianthracite of Late Permian age in the Songzao Coalfield, southwestern China: mineralogical and geochemical relations with underlying mafic tuffs. Int J Coal Geol, 83(4): 430–445

Dai S F, Wang X B, Seredin V V, Hower J C, Ward C R, O'Keefe J M K, Huang W H, Li T, Li X, Liu H D, Xue W, Zhao L (2012a). Petrology, mineralogy, and geochemistry of the Ge-rich coal from the Wulantuga Ge ore deposit, Inner Mongolia, China: new data and genetic implications. Int J Coal Geol, 90–91: 72–99

Dai S F, Xie P P, Jia S H, Ward C R, Hower J C, Yan X Y, French D (2017). Enrichment of U-Re-V-Cr-Se and rare earth elements in the late Permian coals of the Moxinpo Coalfield, Chongqing, China: genetic implications from geochemical and mineralogical data. Ore Geol Rev, 80: 1–17

Dai S F, Yan X Y, Ward C R, Hower J C, Zhao L, Wang X B, Zhao L X, Ren D Y, Finkelman R B (2018). Valuable elements in Chinese coals: a review. Int Geol Rev, 60(5–6): 590–620

Dai S F, Yang J Y, Ward C R, Hower J C, Liu H D, Garrison T M, French D, O'Keefe J M K (2015c). Geochemical and mineralogical evidence for a coal-hosted uranium deposit in the Yili Basin, Xinjiang, northwestern China. Ore Geol Rev, 70: 1–30

Dai S F, Zhang W G, Ward C R, Seredin V V, Hower J C, Li X, Song W J, Wang X B, Kang H, Zheng L C, Wang P P, Zhou D (2013). Mineralogical and geochemical anomalies of late Permian coals from the Fusui Coalfield, Guangxi Province, southern China: influences of terrigenous materials and hydrothermal fluids. Int J Coal Geol, 105: 60–84

Dai S F, Zhou Y P, Zhang M Q, Wang X B, Wang J M, Song X L, Jiang Y F, Luo Y B, Song Z T, Yang Z, Ren D Y (2010a). A new type of Nb(Ta)-Zr(Hf)-REE-Ga polymetallic deposit in the late Permian coal-bearing strata, eastern Yunnan, southwestern China: possible economic significance and genetic implications. Int J Coal Geol, 83(1): 55–63

Ding Z H, Zheng B S, Zhang J, Belkin H E, Finkelman R B, Zhao F, Zhou D, Zhou Y, Chen C (1999). Preliminary study on the mode of occurrence of arsenic in high arsenic coals from southwest Guizhou Province. Sci China Ser D Earth Sci, 42(6): 655–661

Duan P P (2017). Geochemistry of toxic elements in high-sulfur coal from southwestern China and their partitioning during coal preparation. Dissertation for the Doctoral Degree. Xuzhou: China University of Mining and Technology (in Chinese)

Duan P P, Wang W F, Liu X H, Qian F C, Sang S X, Xu S C (2017). Distribution of As, Hg and other trace elements in different size and density fractions of the Reshuihe high-sulfur coal, Yunnan Province, China. Int J Coal Geol, 173: 129–141

Duan P P, Wang W F, Liu X H, Sang S X, Ma M Y, Zhang W (2019). Differentiation of rare earth elements and yttrium in different size and density fractions of the Reshuihe coal, Yunnan Province, China. Int J Coal Geol, 207: 1–11

Elderfield H (1988). The oceanic chemistry of the rare-earth elements. Philos Trans R Soc Lond A, 325(1583): 105–126

Elderfield H, Greaves M J (1981). Negative cerium anomalies in the rare earth element patterns of oceanic ferromanganese nodules.

Earth Planet Sci Lett, 55(1): 163–170

Elderfield H, Greaves M J (1982). The rare earth elements in seawater. Nature, 296(5854): 214–219

Eskenazy G M (1987a). Rare earth elements and yttrium in lithotypes of Bulgarian coals. Org Geochem, 11(2): 83–89

Eskenazy G M (1987b). Rare earth elements in a sampled coal from the Pirin Deposit, Bulgaria. Int J Coal Geol, 7(3): 301–314

Finkelman R B (1993). Trace and minor elements in coal. In: Engel M H, Macko S, eds. Organic Geochemistry. New York: Plenum: 593–607

Fu B, Hower J C, Zhang W C, Luo G Q, Hu H Y, Yao H (2022). A review of rare earth elements and yttrium in coal ash: content, modes of occurrences, combustion behavior, and extraction methods. Pror Energy Combust Sci, 88: 100954

GB/T 482–2008 (2008). Sampling of Coal Seams. Beijing: Chinese Management Committee of Standard Specifications

Goldschmidt V M, Peters C L (1933). Uber die Anreicherung seltener Elemente in Steinkohlen: Nachrichten von der Gesellschaft der Wissenschafter zu Göttingen. Mathematisch-Physikalische Klasse: 371–386

Gromet L P, Haskin L A, Korotev R L, Dymek R F (1984). The "North American shale composite": its compilation, major and trace element characteristics. Geochim Cosmochim Acta, 48(12): 2469–2482

Hower J C, Granite E J, Mayfield D B, Lewis A S, Finkelman R B (2016). Notes on contributions to the science of rare earth element enrichment in coal and coal combustion by-products. Minerals (Basel), 6(2): 32

Hu R Z, Qi H W, Zhou M F, Su W C, Bi X W, Peng J T, Zhong H (2009). Geological and geochemical constraints on the origin of the giant Lincang coal seam-hosted germanium deposit, Yunnan, SW China: a review. Ore Geol Rev, 36(1–3): 221–234

Ketris M P, Yudovich Y E (2009). Estimations of Clarkes for carbonaceous biolithes: world average for trace element contents in black shales and coals. Int J Coal Geol, 78(2): 135–148

Kislyakov Y M, Shchetochkin V N (2000). Hydrogenic Ore Formation. Moscow: Geoinformmark, 608 (in Russian)

Li B Q, Zhuang X G, Li J, Querol X, Font O, Moreno N (2017). Enrichment and distribution of elements in the Late Permian coals from the Zhina Coalfield, Guizhou Province, southwest China. Int J Coal Geol, 171: 111–129

Li B Q, Zhuang X G, Querol X, Moreno N, Cordoba P, Shangguan Y, Yang L J, Li J, Zhang F (2020b). Geological controls on the distribution of REY-Zr (Hf)-Nb (Ta) enrichment horizons in late Permian coals from the Qiandongbei Coalfield, Guizhou Province, SW China. Int J Coal Geol, 231: 103604

Li B Q, Zhuang X G, Querol X, Moreno N, Yang L J, Shangguan Y F, Li J (2019). Mineralogy and geochemistry of Late Permian coals within the Tongzi Coalfield in Guizhou Province, southwest China. Minerals (Basel), 10(1): 44

Li S Y, Bo P H, Kang L W, Guo H G, Gao W Y, Qin S J (2020a). Activation Pretreatment and leaching process of high-alumina coal fly ash to extract lithium and aluminum. Metals (Basel), 10(7): 893

Li X, Dai S F, Nechaev V P, Graham I T, French D, Wang X B, Zhao L, Zhao J T (2021). Mineral matter in the Late Permian C1 coal from Yunnan Province, China, with emphasis on its origins and modes of occurrence. Minerals (Basel), 11(1): 19

Lin R H, Stuckman M, Howard B H, Bank T L, Roth E A, Macala M K, Lopano C, Soong Y, Granite E J (2018). Application of sequential extraction and hydrothermal treatment for characterization and enrichment of rare earth elements from coal fly ash. Fuel, 232: 124–133

Liu J J, Dai S F, Song H J, Nechaev V P, French D, Spiro B F, Graham I T, Hower J C, Shao L Y, Zhao J T (2021). Geological factors controlling variations in the mineralogical and elemental compositions of Late Permian coals from the Zhijin-Nayong Coalfield, western Guizhou, China. Int J Coal Geol, 247: 103855

Liu J J, Nechaev V P, Dai S F, Song H J, Nechaeva E V, Jiang Y F, Graham I T, French D, Yang P, Hower J C (2020). Evidence for multiple sources for inorganic components in the Tucheng coal deposit, western Guizhou, China and the lack of critical-elements. Int J Coal Geol, 223: 103468

Liu J J, Song H J, Dai S F, Nechaev V P, Graham I T, French D, Nechaeva E V (2019). Mineralization of REE-Y-Nb-Ta-Zr-Hf in Wuchiapingian coals from the Liupanshui Coalfield, Guizhou, southwestern China: geochemical evidence for terrigenous input. Ore Geol Rev, 115: 103190

Luo Y B, Zheng M P (2016). Origin of minerals and elements in the Late Permian coal seams of the shiping mine, Sichuan, Southwestern China. Minerals (Basel), 6(3): 74

Ma J L, Xiao L, Zhang K, Jiao Y K, Wang Z Z, Li J X, Guo W M, Gao P P, Qin S J, Zhao C L (2020). Geochemistry of Carboniferous-Permian coal from the Wujiawan Mine, Datong Coalfield, northern China: modes of occurrence, origin of valuable trace elements, and potential industrial utilization. Minerals (Basel), 10(9): 776

Mondal S, Ghar A, Satpati A, Sinharoy P, Singh D K, Sharma J N, Sreenivas T, Kain V (2019). Recovery of rare earth elements from coal fly ash using TEHDGA impregnated resin. Hydrometallurgy, 185: 93–101

Pan J H, Hassas B V, Rezaee M, Zhou C C, Pisupati S V (2021). Recovery of rare earth elements from coal fly ash through sequential chemical roasting, water leaching, and acid leaching processes. J Clean Prod, 284: 124725

Qin S J, Gao K, Sun Y Z, Wang J X, Zhao C L, Li S Y, Lu Q F (2018a). Geochemical characteristics of rare-metal, rare-scattered and rare-earth elements, and minerals in the Late Permian Coals from the Moxinpo Mine, Chongqing, China. Energy Fuels, 32(3): 3138–3151

Qin S J, Lu Q F, Gao K, Bo P H, Wu S H (2018b). Geochemistry of elements associated with Late Permian coal in the Zhongliangshan mine, Chongqing, southwest China. Energy Explor Exploit, 36(6): 1655–1673

Qin S J, Lu Q F, Wu S H, Bo P H (2018c). Organic geochemistry of the Late Permian coal from the Zhongliangshan mine, Chongqing. J China Coal Soc 43(7): 1973–1982 (in Chinese)

Qin S J, Sun Y Z, Li Y H, Wang J X, Zhao C L, Gao K (2015a). Coal deposits as promising alternative sources for gallium. Earth Sci Rev, 150: 95–101

Qin S J, Zhao C L, Li Y H, Zhang Y (2015b). Review of coal as a promising source of lithium. Int J Oil Gas Coal Technol, 9(2):

215–229

Seredin V V (1991). About the new type of rare earth element mineralization in the Cenozoic coal-bearing basins. Dokl Akad Nauk SSSR, 320: 1446–1450

Seredin V V (1996). Rare earth element -bearing coals from Russian Far East deposits. Int J Coal Geol, 30(1–2): 101–129

Seredin V V (2010). A new method for primary evaluation of the outlook for rare earth element ores. Geol Ore Deposits, 52(5): 428–433

Seredin V V, Dai S F (2012). Coal deposits as potential alternative sources for lanthanides and yttrium. Int J Coal Geol, 94: 67–93

Seto M, Akagi T (2008). Chemical condition for the appearance of a negative Ce anomaly in stream waters and groundwaters. Geochem J, 42(4): 371–380

Smith R C, Taggart R K, Hower J C, Wiesner M R, Hsu-Kim H (2019). Selective recovery of rare earth elements from coal fly ash leachates using liquid membrane processes. Environ Sci Technol, 53(8): 4490–4499

Sun Y Z, Zhao C L, Qin S J, Xiao L, Li Z S, Lin M Y (2016). Occurrence of some valuable elements in the unique 'high-aluminium coals' from the Jungar coalfield, China. Ore Geol Rev, 72: 659–668

Sverjensky D A (1984). Europium redox equilibria in aqueous solution. Earth Planet Sci Lett, 67(1): 70–78

Taggart R K, Hower J C, Hsu-Kim H (2018). Effects of roasting additives and leaching parameters on the extraction of rare earth elements from coal fly ash. Int J Coal Geol, 196: 106–114

Tang X Y, Huang W H (2004). Trace elements in Chinese coal. Shanghai: Commercial Press (in Chinese)

Taylor S R, McLennan S H (1985). The Continental Crust: Its Composition and Evolution. Oxford: Blackwell

Wang P P, Yan X Y, Guo W M, Zhang S Y, Wang Z, Xu Y G, Wang L (2016). Geochemistry of trace elements in coals from the Yueliangtian Mine, Western Guizhou, China: abundances, modes of occurrence, and potential industrial utilization. Energy Fuels, 30(12): 10268–10281

Wang Z, Dai S F, Zou J H, French D, Graham I T (2019). Rare earth elements and yttrium in coal ash from the Luzhou power plant in Sichuan, Southwest China: concentration, characterization and optimized extraction. Int J Coal Geol, 203: 1–14

Xiao L, Xu Y G, Mei H J, Zheng Y F, He B, Pirajno F (2004). Distinct mantle sources of low-Ti and high-Ti basalts from the western Emeishan large igneous province, SW China: implications for plume–lithosphere interaction. Earth Planet Sci Lett, 228(3–4): 525–546

Xin L, Wang Z T, Wang G, Nie W, Zhou G, Cheng W M, Xie J (2017). Technological aspects for underground coal gasification in steeply inclined thin coal seams at Zhongliangshan coal mine in China. Fuel, 191: 486–494

Xu F, Qin S J, Li S Y, Wang J X, Qi D E, Lu Q F, Xing J K (2022). Distribution, occurrence mode, and extraction potential of critical elements in coal ashes of the Chongqing Power Plant. J Clean Prod, 342: 130910

Yan X Y, Dai S F, Graham I T, He X, Shan K H, Liu X (2018). Determination of Eu concentrations in coal, fly ash and sedimentary rocks using a cation exchange resin and inductively coupled plasma mass spectrometry (ICP-MS). Int J Coal Geol, 191: 152–156

Zhang W C, Honaker R (2020). Process development for the recovery of rare earth elements and critical metals from an acid mine leachate. Miner Eng, 153: 106382

Zhao C L, Duan D J, Li Y H, Zhang J Y (2012). Rare earth elements in No. 2 coal of Huangling mine, Huanglong coalfield, China. Energy Explor Exploit, 30(5): 803–818

Zhao Y Y, Zeng F G, Liang H Z, Tang Y G, Li M F, Xiang J H, Wen X T (2017). Chromium and vanadium bearing nanominerals and ultra-fine particles in a super-high-organic-sulfur coal from Ganhe coalmine, Yanshan Coalfield, Yunnan, China. Fuel, 203: 832–842

Zhuang X G, Querol X, Alastuey A, Juan R, Plana F, Lopez-Soler A, Du G, Martynov V V (2006). Geochemistry and mineralogy of the Cretaceous Wulantuga high-germanium coal deposit in Shengli coal field, Inner Mongolia, Northeastern China. Int J Coal Geol, 66(1–2): 119–136

Zhuang X G, Querol X, Alastuey A, Plana F, Moreno N, Andres J M, Wang H L (2007). Mineralogy and geochemistry of the coals from the Chongqing and Southeast Hubei coal mining districts, South China. Int J Coal Geol, 71(2–3): 263–275

Zou J H, Cheng L F, Guo Y C, Wang Z C, Tian H M, Li T (2020). Mineralogical and geochemical characteristics of lithium and rare earth elements in high-sulfur coal from the Donggou Mine, Chongqing, Southwestern China. Minerals (Basel), 10(7): 627

Zou J H, Han F, Li T, Tian H M, Li Y J (2018). Mineralogical and geochemical compositions of the Lopingian Coals in the Zhongliangshan Coalfield, Southwestern China. Minerals (Basel), 8(3): 104

Table S1 The proximate and sulfur analysis (%), and the major elemental oxides (%), and Ba and Zr (μg/g) contents in the Zhongliangshan coal

Samples	M_{ad}	V_{daf}	A_d	$S_{t,d}$	$S_{p,d}$	$S_{s,d}$	$S_{o,d}$	SiO_2	Al_2O_3	Fe_2O_3	CaO	TiO_2	MgO	K_2O	Na_2O	P_2O_5	MnO	Ba	Zr
ZLS-R	1.96	46.96	67.93	10.42	6.50	0.82	3.10	34.90	15.16	10.82	0.73	1.83	0.608	1.545	1.006	0.1112	0.0543	243.9	557.4
ZLS-1	1.09	26.47	26.79	7.16	4.19	0.58	2.40	12.53	6.72	6.78	0.56	0.45	0.211	0.299	0.186	0.0188	0.0178	82.52	124.6
ZLS-2	0.96	23.47	15.45	2.52	1.87	0.12	0.53	7.76	4.72	1.90	0.60	0.27	0.118	0.101	0.075	0.0073	0.0043	43.30	67.01
ZLS-3	0.98	22.48	12.32	2.29	1.87	0.04	0.38	6.19	4.52	1.50	0.35	0.14	0.093	0.049	0.054	0.0068	0.0022	27.69	39.89
ZLS-4	0.84	21.73	10.29	1.62	1.13	0.003	0.49	4.95	3.84	1.04	0.31	0.13	0.071	0.038	0.041	0.0061	0.0015	24.33	36.82
ZLS-5	0.79	23.11	9.78	0.81	0.60	0.08	0.13	4.54	3.55	0.17	0.66	0.25	0.069	0.046	0.038	0.0062	0.0021	21.70	58.30
ZLS-6	0.83	22.57	10.49	1.40	0.64	0.11	0.35	5.34	4.18	0.32	0.21	0.24	0.096	0.101	0.048	0.0072	0.0011	32.90	71.86
ZLS-7	0.81	21.94	10.99	1.49	0.69	0.02	0.78	5.37	4.44	0.77	0.21	0.18	0.094	0.091	0.041	0.0078	0.0013	41.30	60.28
ZLS-8	0.88	24.26	14.23	1.70	1.06	0.01	0.63	6.06	5.02	1.08	1.41	0.19	0.128	0.111	0.051	0.0089	0.0055	68.97	66.97
ZLS-9	0.84	23.88	22.29	4.45	2.17	0.66	1.63	10.54	8.56	2.93	0.26	0.55	0.276	0.462	0.092	0.0164	0.0026	86.12	126.9
ZLS-10	0.74	20.87	10.98	1.55	0.89	0.01	0.65	5.18	4.46	0.84	0.24	0.21	0.071	0.062	0.040	0.0203	0.0017	36.59	68.23
ZLS-11	0.72	22.47	10.37	1.36	0.62	0.01	0.73	4.69	4.05	0.58	0.39	0.22	0.068	0.058	0.032	0.0102	0.0024	26.72	73.75
ZLS-12	0.83	21.70	14.12	1.32	0.66	0.001	0.66	6.88	5.60	0.55	0.21	0.48	0.117	0.168	0.060	0.0112	0.0015	36.33	124.2
ZLS-13	0.92	21.71	15.62	1.11	0.42	0.001	0.69	7.76	6.46	0.44	0.19	0.33	0.135	0.178	0.057	0.0108	0.0038	58.94	109.2
ZLS-14	0.86	19.63	10.49	1.00	0.54	0.01	0.45	5.06	4.27	0.16	0.27	0.19	0.067	0.051	0.037	0.0097	0.0014	41.26	63.13
ZLS-15	0.76	21.12	9.17	0.88	0.16	0.001	0.72	4.20	3.56	0.19	0.51	0.14	0.059	0.041	0.031	0.0076	0.0031	29.66	61.33
ZLS-16	0.78	20.97	9.07	1.15	0.56	0.01	0.58	4.29	3.67	0.32	0.31	0.14	0.058	0.047	0.033	0.0069	0.0017	41.26	60.12
ZLS-17	1.04	25.52	29.00	3.41	2.67	0.18	0.55	13.56	11.14	3.13	0.37	0.99	0.319	0.382	0.109	0.0246	0.0067	109.5	189.9
ZLS-18	1.10	25.79	31.75	7.75	5.26	1.37	1.12	13.88	12.04	7.92	0.13	0.86	0.333	0.355	0.117	0.0221	0.0079	87.26	133.5
ZLS-19	1.06	22.69	20.21	7.05	4.90	1.09	1.06	8.84	7.92	4.36	0.29	0.64	0.151	0.089	0.088	0.0157	0.0033	71.09	137.8
ZLS-P	1.93	38.99	60.98	3.55	3.06	0.18	0.31	28.02	23.66	3.88	0.15	4.28	0.426	0.193	0.319	0.0508	0.0033	45.54	603.9
ZLS-20	0.76	20.03	11.08	3.24	2.13	0.10	1.01	5.26	4.53	0.83	0.19	0.23	0.074	0.060	0.037	0.0121	0.0014	23.96	61.93
ZLS-21	0.87	20.64	11.80	1.46	0.78	0.06	0.62	5.44	5.07	1.67	0.18	0.21	0.060	0.033	0.037	0.0105	0.0021	19.68	55.93
Average	0.88	22.53	15.06	2.61	1.61	0.21	0.77	7.06	5.63	1.78	0.37	0.34	0.13	0.13	0.06	0.012	0.004	48.15	85.32